

1 **A Computational Approach for the Identification of Novel L1 Transcriptional** 2 **Regulators**

3 Juan I. Bravo^{1,2}, Chanelle R. Mizrahi^{1,3}, Seungsoo Kim⁴, Lucia Zhang^{1,5}, Yousin Suh^{4,6}, Bérénice
4 A. Benayoun^{1,7,8,9,10}

5 ¹ Leonard Davis School of Gerontology, University of Southern California, Los Angeles, CA
6 90089, USA.

7 ² Graduate program in the Biology of Aging, University of Southern California, Los Angeles, CA
8 90089, USA.

9 ³ USC Gerontology Enriching MSTEM to Enhance Diversity in Aging Program, University of
10 Southern California, Los Angeles, CA 90089, USA.

11 ⁴ Department of Obstetrics and Gynecology, Columbia University Irving Medical Center, New
12 York, NY 10032, USA.

13 ⁵ Quantitative and Computational Biology Department, USC Dornsife College of Letters, Arts
14 and Sciences, Los Angeles, CA 90089, USA.

15 ⁶ Department of Genetics and Development, Columbia University Irving Medical Center, New
16 York, NY 10032, USA.

17 ⁷ Molecular and Computational Biology Department, USC Dornsife College of Letters, Arts and
18 Sciences, Los Angeles, CA 90089, USA.

19 ⁸ Biochemistry and Molecular Medicine Department, USC Keck School of Medicine, Los
20 Angeles, CA 90089, USA.

21 ⁹ USC Norris Comprehensive Cancer Center, Epigenetics and Gene Regulation, Los Angeles,
22 CA 90089, USA.

23 ¹⁰ USC Stem Cell Initiative, Los Angeles, CA 90089, USA.

24

25 **KEYWORDS:** LINE1, transposons, regulators, eQTLs, screen, aging, GWAS

26 **ABSTRACT**

27 Long interspersed element 1 (L1) are a family of autonomous, actively mobile
28 transposons that occupy ~17% of the human genome. The pleiotropic effects L1
29 induces in host cells—promoting genome instability, inflammation, or cellular
30 senescence—are established, and L1's associations with aging and aging diseases are
31 widely recognized. However, because of the cell type-specific nature of transposon
32 control, the catalogue of L1 regulators remains incomplete.

33 Here, we employ an eQTL approach leveraging transcriptomic and genomic data from
34 the GEUVADIS and 1000Genomes projects to computationally identify new candidate
35 regulators of L1 expression in lymphoblastoid cell lines. To cement the role of candidate
36 genes in L1 regulation, we experimentally modulate the levels of top candidates *in vitro*,
37 including *IL16*, *STARD5*, *HSDB17B12*, and *RNF5*, and assess changes in TE family
38 expression by Gene Set Enrichment Analysis (GSEA). Remarkably, we observe subtle
39 but widespread upregulation of TE family expression following *IL16* and *STARD5*
40 overexpression. Moreover, a short-term 24 hour exposure to recombinant human IL16
41 was sufficient to transiently induce subtle but widespread upregulation of *L1*
42 subfamilies. Finally, we find that many L1 expression-associated genetic variants are
43 co-associated with aging traits across genome-wide association study databases.

44 Our results expand the catalogue of genes implicated in L1 transcriptional control and
45 further suggest that L1 contributes to aging processes. Given the ever-increasing
46 availability of paired genomic and transcriptomic data, we anticipate this new approach
47 to be a starting point for more comprehensive computational scans for transposon
48 transcriptional regulators.

49 **BACKGROUND**

50 Transposable elements (TEs) constitute ~45% of the human genome [1]. Among
51 these, the long interspersed element-1 (LINE-1 or L1) family of transposons is the most
52 abundant, accounting for ~16-17% [1, 2], and remains autonomously mobile, with
53 humans harboring an estimated 80-100 retrotransposition-competent L1 copies [3].
54 These retrotransposition competent L1s belong to evolutionarily younger L1PA and
55 L1Hs subfamilies, are ~6 kilobases long, carry an internal promoter in their 5'-
56 untranslated region (UTR), and encode two proteins — L1ORF1p and L1ORF2p — that
57 are necessary for transposition [4]. The remaining ~500,000 copies are non-
58 autonomous or immobile because of the presence of inactivating mutations or
59 truncations [1] and include L1 subfamilies of all evolutionary ages, including the
60 evolutionarily older L1P and L1M subfamilies. Though not all copies are transposition
61 competent, L1s can nevertheless contribute to aspects of aging [5, 6] and aging-
62 associated diseases [7-10].

63 Though mechanistic studies characterizing the role of L1 in aging and aging-
64 conditions are limited, it is clear that its effects are pleiotropic. L1 can contribute to
65 genome instability via insertional mutagenesis and an expansion of copy number with
66 age [11] and during senescence [12]. L1 can also play a contributing role in shaping
67 inflammatory and cellular senescence phenotypes. The secretion of a panoply of pro-
68 inflammatory factors is a marker of senescent cells, called the senescence associated
69 secretory phenotype (SASP) [13]. Importantly, the SASP is believed to stimulate the
70 innate immune system and contribute to chronic, low-grade, sterile inflammation with
71 age, a phenomenon referred to as “inflamm-aging” [13, 14]. During deep senescence,

72 L1 are transcriptionally de-repressed and consequently generate cytosolic DNA that
73 initiates an immune response consisting of the production and secretion of pro-
74 inflammatory interferons [15]. Finally, L1 is causally implicated in aging-associated
75 diseases like cancer. L1 may contribute to cancer by (i) serving as a source for
76 chromosomal rearrangements that can delete tumor-suppressor genes [16] or (ii)
77 introducing its promoter into normally-silenced oncogenes [17]. Thus, because of the
78 pathological effects L1 can have on hosts, it is critical that hosts maintain precise control
79 over L1 activity.

80 Eukaryotic hosts have evolved several pre- and post-transcriptional mechanisms
81 for regulating TEs [18, 19]. Nevertheless, our knowledge of regulatory genes remains
82 incomplete because of cell type-specific regulation and the complexity of methods
83 required to identify regulators. Indeed, one clustered regularly interspaced short
84 palindromic repeats (CRISPR) screen in two cancer cell lines for regulators of L1
85 transposition identified >150 genes involved in diverse biological functions, such as
86 chromatin regulation, DNA replication, and DNA repair [20]. However, only about ~36%
87 of the genes identified in the primary screen exerted the same effects in both cell lines
88 [20], highlighting the cell type-specific nature of L1 control. Moreover, given the
89 complexities of *in vitro* screens, especially in non-standard cell lines or primary cells, *in*
90 *silico* screens for L1 regulators may facilitate the task of identifying and cataloguing
91 candidate regulators across cell and tissue types. One such attempt was made by
92 generating gene-TE co-expression networks from RNA sequencing (RNA-seq) data
93 generated from multiple tissue types of cancerous origin [21]. Although co-expression
94 modules with known TE regulatory functions, such as interferon signaling, were

95 correlated with TE modules, it is unclear whether other modules may harbor as of now
96 uncharacterized TE-regulating properties, since no validation experiments were carried
97 out. Additionally, this co-expression approach is limited, as no mechanistic directionality
98 can be assigned between associated gene and TE clusters, complicating the
99 prioritization of candidate regulatory genes for validation. Thus, there is a need for the
100 incorporation of novel “omic” approaches to tackle this problem. Deciphering the
101 machinery that controls TE activity in healthy somatic cells will be crucial, in order to
102 identify checkpoints lost in diseased cells.

103 The 1000Genomes Project and GEUVADIS Consortium provide a rich set of
104 genomic resources to explore the mechanisms of human TE regulation *in silico*. Indeed,
105 the 1000Genomes project generated a huge collection of genomic data from thousands
106 of human subjects across the world, including single nucleotide variant (SNV) and
107 structural variant (SV) data [22, 23]. To accomplish this, the project relied on
108 lymphoblastoid cell lines (LCLs), which are generated by infecting resting B-cells in
109 peripheral blood with Epstein-Barr virus (EBV). Several properties make them
110 advantageous for use in large-scale projects, e.g. they can be generated relatively
111 uninvvasively, they provide a means of obtaining an unlimited amount of a subject’s DNA
112 and other biomolecules, and they can serve as an *in vitro* model for studying the effects
113 of genetic variation with any phenotype of interest [24, 25]. Indeed, the GEUVADIS
114 Consortium generated transcriptomic data for a subset of subjects sampled by the
115 1000Genomes Project, and used their genomic data to define the effects genetic
116 variation on gene expression [26]. Together, these resources provide a useful toolkit for
117 investigating the genetic regulation of TEs, generally, and L1, specifically.

118 In this study, we (i) develop a pipeline to identify novel candidate regulators of L1
119 expression in lymphoblastoid cell lines, (ii) provide experimental evidence for the
120 involvement of top candidates in L1 expression control, and (iii) expand and reinforce
121 the catalogue of diseases linked to L1.

122

123

124 RESULTS

125

126 *In silico scanning for L1 subfamily candidate regulators by eQTL analysis*

127 To identify new candidate regulators of L1 transcription, we decided to leverage
128 publicly available human “omic” datasets with both genetic and transcriptomic
129 information. For this analysis, we focused on samples for which the following data was
130 available: (i) mRNA-seq data from the GEUVADIS project, (ii) SNVs called from whole-
131 genome sequencing data overlaid on the hg38 human reference genome made
132 available by the 1000Genomes project, and (iii) repeat structural variation data made
133 available by the 1000Genomes project. This yielded samples from 358 European and
134 86 Yoruban individuals, all of whom declared themselves to be healthy at the time of
135 sample collection (**Figure 1A**). Using the GEUVADIS data, we obtained gene and TE
136 subfamily expression counts using TETranscripts [27]. As a quality control step, we
137 checked whether mapping rates segregated with ancestry groups, which may bias
138 results. However, the samples appeared to cluster by laboratory rather than by ancestry
139 (**Figure S1A**). As additional quality control metrics, we also checked whether the SNV
140 and SV data segregated by ancestry following principal component analysis (PCA).
141 These analyses demonstrated that the top two and the top three principal components
142 from the SNV and SV data, respectively, segregated ancestry groups (**Figure S1B**,
143 **Figure S1C**).

144

145 We then chose to do a three-part integration of the available “omic” data (**Figure**
146 **1B**). Since TETranscripts quantifies TE expression aggregated at the TE subfamily level

147 and discards TE position information, we chose to carry out a *trans*-eQTL analysis
148 against global expression of each L1 subfamily. We reasoned that there would have to
149 be factors (i.e., miRNAs, proteins, non-coding RNAs) mediating the effects of SNVs on
150 L1 subfamily expression. Thus, to identify candidate genic mediators, we searched for
151 genes with *cis*-eQTLs that overlapped with L1 *trans*-eQTLs. As a final filter, we
152 reasoned that for a subset of regulators, L1 subfamily expression would respond to
153 changes in the expression of those regulators. Consequently, we chose to quantify the
154 association between L1 subfamily expression and candidate gene expression by linear
155 regression. We hypothesized that this three-part integration would result in
156 combinations of significantly correlated SNVs, genes, and L1 subfamilies (**Figure 1B**).

157

158 The *trans*-eQTL analysis against every expressed L1 subfamily led to the
159 identification of 499 *trans*-eQTLs distributed across chromosomes 6, 11, 12, 14, and 15
160 that passed genome-wide significance (**Figure 1C, Supplementary Table S1A**). The
161 *cis*-eQTL analysis led to the identification of 845,260 *cis*-eQTLs that passed genome-
162 wide significance (**Supplementary Figure S2, Supplementary Table S1B**). After
163 integrating the identified *cis*- and *trans*-eQTLs and running linear regression, we
164 identified 1,272 SNV-Gene-L1 trios that fulfilled our three-part integration approach
165 (**Supplementary Table S1C**). Among this pool of trios, we identified 7 unique protein-
166 coding genes including *IL16*, *STARD5*, *HLA-DRB5*, *HLA-DQA2*, *HSD17B12*, *RNF5*, and
167 *FKBPL* (**Figure 1C**). We note that although *EHMT2* did not pass out screening
168 approach, it does overlap *EHMT2-AS1*, which did pass our screening thresholds
169 (**Figure 1C**). We also note that several other unique non-coding genes, often

170 overlapping the protein-coding genes listed, were also identified (**Figure 1C**). For
171 simplicity of interpretation, we focused on protein-coding genes during downstream
172 experimental validation.

173

174 Next, to define first and second tier candidate regulators, we clumped SNVs in
175 linkage disequilibrium (LD) by L1 *trans*-eQTL p-value to identify the most strongly
176 associated genetic variant in each genomic region (**Figure 2A, Supplementary Figure**
177 **S3A**). LD-clumping identified the following index SNVs (*i.e.* the most strongly associated
178 SNVs in a given region): rs11635336 on chromosome 15, rs9271894 on chromosome
179 6, rs1061810 on chromosome 11, rs112581165 on chromosome 12, and rs72691418
180 on chromosome 14 (**Supplementary Table S1D**). Genes linked to these SNVs were
181 considered first tier candidate regulators and included *IL16*, *STARD5*, *HLA-DRB5*, *HLA-*
182 *DQA2*, and *HSD17B12* (**Figure 2B, Supplementary Table S1E**). The remaining genes
183 were linked to clumped, non-index SNVs and were consequently considered second tier
184 candidates and included *RNF5*, *EHMT2-AS1*, and *FKBPL* (**Supplementary Figure**
185 **S3B**). Additionally, for simplicity of interpretation, we considered only non-*HLA* genes
186 during downstream experimental validation, since validation could be complicated by
187 the highly polymorphic nature of *HLA* loci [28] and their involvement in multi-protein
188 complexes.

189

190 Finally, to computationally determine whether candidate genes may causally
191 influence L1 subfamily expression, we carried out mediation analysis on all SNV-gene-
192 L1 trios (**Supplementary Figure S4A**). Interestingly, 868 out of the 1,272 (68.2%) trios

193 exhibited significant (FDR < 0.05) mediation effects (**Supplementary Table S1F**).
194 Among the 1st tier candidate regulators, significant, partial, and consistent mediation
195 effects could be attributed to *STARD5*, *IL16*, *HSD17B12*, and *HLA-DRB5*
196 (**Supplementary Figure S4B, Supplementary Table S1F**). To note, while significant
197 mediation could be attributed to the index SNV for *STARD5*, significant mediation could
198 only be attributed to clumped SNVs for *IL16* and *HSD17B12*. Given that *STARD5* and
199 *IL16* share *cis*-eQTL SNVs, this suggests that *STARD5* may be the more potent
200 mediator. Among the 2nd tier candidate regulators, significant, partial, and consistent
201 mediation effects could be attributed to *RNF5*, *EHMT2-AS1*, and *FKBP1*
202 (**Supplementary Figure S4C, Supplementary Table S1F**). These results suggest that
203 candidate genes may mediate the effects between linked SNVs and L1 subfamilies.

204

205

206 *In silico scanning for L1 subfamily candidate regulators in an African population*

207 We next sought to assess the cross-ancestry regulatory properties of candidate
208 genes by repeating our scan using the Yoruban samples as a smaller but independent
209 replication cohort. Here, rather than conduct a genome-wide scan for *cis*- and *trans*-
210 associated factors, we opted for a targeted approach focusing only on gene *cis*-eQTLs
211 and L1 subfamily *trans*-eQTLs that were significant in the analysis with European
212 samples (**Supplementary Figure S5A**). The targeted *trans*-eQTL analysis led to the
213 identification of 227 significant (FDR < 0.05) *trans*-eQTLs distributed across
214 chromosomes 6 and 11 (**Supplementary Table S2A**). The targeted *cis*-eQTL analysis
215 led to the identification of 1,248 significant (FDR < 0.05) *cis*-eQTLs (**Supplementary**

216 **Table S2B**). After integrating the identified *cis*- and *trans*-eQTLs and running linear
217 regression, we identified 393 SNV-Gene-L1 trios that fulfilled our three-part integration
218 approach (**Supplementary Table S2C**). Among this pool of trios, we identified 2 unique
219 protein-coding genes—*HSD17B12* and *HLA-DRB6*—as well as several unique non-
220 coding genes (**Supplementary Table S2C**). Again, we clumped SNVs in linkage
221 disequilibrium (LD) by L1 *trans*-eQTL p-value. LD-clumping identified the following index
222 SNVs: rs2176598 on chromosome 11 and rs9271379 on chromosome 6
223 (**Supplementary Table S2D**). Genes linked to these SNVs were considered first tier
224 candidate regulators and included both *HSD17B12* and *HLA-DRB6* (**Supplementary**
225 **Figure S5B, Supplementary Table S2E**). Finally, we carried out mediation analysis on
226 all SNV-gene-L1 trios; however, no significant (FDR < 0.05) mediation was observed
227 (**Supplementary Table S2F**). These results implicate *HSD17B12* and the *HLA* loci as
228 candidate, cross-ancestry L1 expression regulators.

229

230 To assess why some candidate genes did not replicate in the Yoruba cohort, we
231 manually inspected *cis*- and *trans*-eQTL results for trios with those genes
232 (**Supplementary Figure S6A**). Interestingly, we identified rs9270493 and rs9272222 as
233 significant (FDR < 0.05) *trans*-eQTLs for L1MEb expression. However, those SNVs
234 were not significant *cis*-eQTLs for *RNF5* and *FKBP1* expression, respectively. For trios
235 involving *STARD5*, *IL16*, and *EHMT2-AS1*, neither the *cis*-eQTL nor the *trans*-eQTL
236 were significant. We note that for most of these comparisons, although the two
237 genotypes with the largest sample sizes were sufficient to establish a trending change
238 in *cis* or *trans* expression, this trend was often broken by the third genotype with

239 spurious sample sizes. This suggests that replication in the Yoruba cohort may be
240 limited by the small cohort sample size in the GEUVADIS project.

241

242

243 *TE families and known TE-associated pathways are differentially regulated across L1*
244 *trans-eQTL variants*

245 Though our eQTL analysis identified genetic variants associated with the
246 expression of specific, evolutionarily older L1 subfamilies, we reasoned that there may
247 be more global but subtle differences in TE expression profiles among genotype groups,
248 given that TE expression is highly correlated [21]. Thus, for each gene-associated index
249 SNV identified in the European eQTL analysis, we carried out differential expression
250 analysis for all expressed genes and TEs (**Supplementary Table S3A-S3C; Figure**
251 **3A**). At the individual gene level, we detected few significant (FDR < 0.05) changes: 4
252 genes/TEs varied with rs11635336 genotype (*IL16/STARD5*), 4 genes/TEs varied with
253 rs9271894 genotype (*HLA*), and 5 gene/TEs varied with rs1061810 genotype
254 (*HSD17B12*) (**Supplementary Table S3A-S3C**). Importantly, however, these
255 genes/TEs overlapped the genes/TEs identified in the *cis*- and *trans*-eQTL analyses,
256 providing an algorithmically independent link among candidate SNV-gene-TE trios.

257 In contrast to gene-level analyses, Gene Set Enrichment Analysis (GSEA)
258 provides increased sensitivity to subtle but consistent/widespread transcriptomic
259 changes at the level of gene sets (e.g. TE families, biological pathways, etc.). Thus, we
260 leveraged our differential expression analysis in combination with GSEA to identify
261 repeat family and biological pathway gene sets impacted by SNV genotype in the

262 GEUVADIS dataset (**Supplementary Table S3D-S3O; Figure 3A**). Interestingly,
263 changes in the genotype of rs11635336 (*IL16/STARD5*), rs9271894 (*HLA*), and
264 rs1061810 (*HSD17B12*) were associated with an upregulation, upregulation, and
265 downregulation, respectively, of multiple TE family gene sets (**Figure 3B,**
266 **Supplementary Table S3P**). Differentially regulated TE family gene sets included DNA
267 transposons, such as the hAT-Charlie family, and long terminal repeat (LTR)
268 transposons, such as the endogenous retrovirus-1 (ERV1) family (**Figure 3B,**
269 **Supplementary Table S3P**). Noteworthy, the L1 family gene set was the only TE gene
270 set whose expression level was significantly altered across all three SNV analyses
271 (**Figure 3B, Supplementary Table S3P**). Consistent with their relative significance in
272 the L1 *trans*-eQTL analysis, the L1 family gene set was most strongly upregulated by
273 alternating the *IL16/STARD5* SNV (NES = 3.74, FDR = 6.43E-41), intermediately
274 upregulated by alternating the *HLA* SNV (NES = 1.90, FDR = 7.19E-5), and least
275 strongly changed by alternating the *HSD17B12* SNV (NES = -1.57, FDR = 2.11E-2)
276 (**Figure 3C**). We briefly note here that rs9270493, a clumped SNV linked to *RNF5*, was
277 also linked to upregulation of the L1 family gene set (**Supplementary Table S3Q-S3R**).
278 These results suggest that TE subfamily *trans*-eQTLs are associated with subtle but
279 global differences in TE expression beyond a lone TE subfamily.

280

281 Next, we asked if other biological pathways were regulated concomitantly with
282 TE gene sets in response to gene-linked index SNVs, reasoning that such pathways
283 would act either upstream (as regulatory pathways) or downstream (as response
284 pathways) of TE alterations. GSEA with the MSigDB Hallmark pathway gene sets [29,

285 30] identified 5 gene sets fitting this criterion, including “oxidative phosphorylation”,
286 “mTORC1 signaling”, “fatty acid metabolism”, “adipogenesis”, and “cholesterol
287 homeostasis” (**Figure 3D, Supplementary Table S3S**). Interestingly, several of these
288 pathways or genes in these pathways have been implicated in TE regulation before.
289 Rapamycin, which acts through mTORC1, has been shown to alter the expression of L1
290 and other repeats [31, 32]. Estrogens, which are involved in cholesterol and lipid
291 metabolism, have been found to drive changes in repeat expression, and the receptors
292 for both estrogens and androgens are believed to bind repeat DNA [32, 33].
293 Pharmacological inhibition of the mitochondrial respiratory chain and pharmacological
294 reduction of endogenous cholesterol synthesis have also been shown to induce
295 changes in L1 protein levels or repeat expression more broadly [34, 35]. GSEA with the
296 GO Biological Process gene sets (**Figure 3E, Supplementary Table S3T**) and the
297 Reactome gene sets (**Figure 3F, Supplementary Table S3U**) also identified several
298 metabolism-related pathways including “ATP metabolic process”, “Generation of
299 precursor metabolites and energy”, and “metabolism of amino acids and derivatives”.
300 These results add to the catalogue of pathways associated with differences in L1
301 expression.

302

303 In our eQTL analysis, we also identified two orphan index SNVs, rs112581165
304 and rs72691418, to which we could not attribute a protein-coding gene mediator. To
305 determine whether these SNVs also regulate any transposon families or biological
306 pathways, we repeated the differential expression analysis (with all expressed genes
307 and TEs) (**Supplementary Table S4A-S4B**) and the GSEA (**Supplementary Table**

308 **S4C-S4J**) with these SNVs (**Supplementary Figure S7A**). At the individual gene level,
309 we detected 3193 genes/TEs that varied significantly (FDR < 0.05) with rs112581165
310 genotype and 1229 genes/TEs that varied significantly with rs72691418 genotype
311 (**Supplementary Table S4A-S4B**). Similar to above, we next carried out GSEA to
312 identify changes in functionally relevant gene sets. Like the gene-linked index SNVs,
313 changes in the genotype of rs112581165 and rs72691418 were both associated with a
314 downregulation and upregulation, respectively, of 10 TE families (**Supplementary**
315 **Figure S7B, Supplementary Table S4K**). Noteworthy, the L1 family gene set was
316 among the most strongly dysregulated TE family gene sets for both rs112581165 (NES
317 = -4.32, FDR = 5.18E-89) and rs72691418 (NES = 4.01, FDR = 5.38E-79)
318 (**Supplementary Figure S7C**). These results suggest that TE subfamily *trans*-eQTLs
319 are associated with subtle differences in TE expression beyond the lone TE subfamily,
320 even in the absence of a protein-coding gene *cis*-eQTL.

321

322 Like before, we asked if other biological pathways were regulated concomitantly
323 with TE gene sets in response to orphan index SNVs. The top 10 Hallmark pathway
324 gene sets identified by GSEA included gene sets that were previously identified
325 (“oxidative phosphorylation”, “fatty acid metabolism”, and “mTORC1 signaling”), as well
326 as several new pathways (**Supplementary Figure S7D, Supplementary Table S4L**).
327 Among the new pathways, “DNA repair” [20] and the “P53 pathway” [36, 37] have also
328 been linked to L1 control, and proteins in the “Myc targets v1” gene set interact with L1
329 ORF1p [38]. GSEA with the GO Biological Process gene sets (**Supplementary Figure**
330 **S7E, Supplementary Table S4M**) and the Reactome gene sets (**Supplementary**

331 **Figure S7F, Supplementary Table S4N)** identified several metabolism-related
332 pathways and several translation-related pathways, such as “cytoplasmic translation”,
333 “eukaryotic translation initiation”, and “eukaryotic translation elongation”. Importantly,
334 proteins involved in various aspects of proteostasis have been shown to be enriched
335 among L1 ORF1p-interacting proteins [38]. Again, these results add to the catalogue of
336 pathways associated with differences in TE expression, even in the absence of a
337 candidate *cis* mediator.

338

339

340 *Modulation of top candidate gene activity in a lymphoblastoid cell line induces small but*
341 *widespread TE expression changes*

342 We decided to validate the L1 regulatory properties of top candidate genes
343 associated with L1 *trans*-eQTLs. For experimental purposes, we selected the GM12878
344 lymphoblastoid cell line, because (i) it is of the same cell type as the transcriptomic data
345 used here for our eQTL analysis, and (ii) its epigenomic landscape and culture
346 conditions have been well well-characterized as part of the ENCODE project [39, 40].
347 For validation purposes, we selected *IL16*, *STARD5*, *HSD17B12*, and *RNF5* out of the 7
348 protein-coding gene candidates. We chose these genes for validation because the first
349 3 are associated with top *trans*-eQTL SNVs and the fourth one had very strong
350 predicted mediation effects. To note, although GM12878 was part of the 1000Genomes
351 Project, it was not included in the GEUVADIS dataset. However, based on its genotype,
352 we can predict the relative expression of candidate regulators (**Supplementary Figure**
353 **S8A**), which suggest that GM12878 may be most sensitive to modulations in *IL16* and

354 *STARD5* expression, given their relatively low endogenous expression. Interestingly,
355 examination of the ENCODE epigenomic data in GM12878 cells [39] demonstrated that
356 the region near the *IL16/STARD5*-linked index SNV (rs11635336) was marked with
357 H3K4Me1 and H3K27Ac, regulatory signatures of enhancers (**Supplementary Figure**
358 **S8C**). Similarly, the region near the *HLA*-linked index SNV (rs9271894) was marked
359 with H3K4Me1, marked with H3K27Ac, and accessible by DNase, suggesting regulatory
360 properties of the region as an active enhancer (**Supplementary Figure S8C**). These
361 results further highlight the regulatory potential of the *IL16*-, *STARD5*-, and *HLA*-linked
362 SNVs.

363

364 First, we decided to test the transcriptomic impact of overexpressing our top
365 candidates in GM12878 LCLs. Cells were electroporated with overexpression plasmids
366 (or corresponding empty vector), and RNA was isolated after 48h (**Figure 4A,**
367 **Supplementary Figure S9A**). Differential expression analysis comparing control and
368 overexpression samples confirmed the overexpression of candidate genes
369 (**Supplementary Figure S9B, Supplementary Table S5A-S5D**). Intriguingly, we
370 observed that *IL16* was significantly upregulated following *STARD5* overexpression
371 (**Supplementary Figure S9C, Supplementary Table S5B**), although the inverse was
372 not observed (**Supplementary Figure S9C, Supplementary Table S5A**), suggesting
373 that *IL16* may act downstream of *STARD5*. We note here that, consistent with the use
374 of a high expression vector, the *IL16* upregulation elicited by *STARD5* overexpression
375 (\log_2 fold change = 0.45) was weaker than the upregulation from the *IL16*
376 overexpression (\log_2 fold change = 1.89) (**Supplementary Table S5A-S5B**).

377

378 To further assess the biological relevance of each overexpression, we carried out
379 GSEA using the GO Biological Process, Reactome pathway, and Hallmark pathway
380 gene sets (**Supplementary Table S5E-S5P**). Importantly, GSEA using GO Biological
381 Process and Reactome pathway gene sets highlighted differences that were consistent
382 with the known biology of our candidate genes. Firstly, *IL16* is involved in regulating T-
383 cell activation, B-cell differentiation, and functions as a chemoattractant [41-46].
384 Moreover, it modulates macrophage polarization by regulating *IL-10* expression [47].
385 *IL16* overexpressing cells showed upregulation for “phagocytosis recognition” and
386 “positive chemotaxis”, downregulation for “negative regulation of cell differentiation”, and
387 downregulation for “Interleukin 10 signaling” (**Figure 4B-4C**). Secondly, *STARD5*
388 encodes a cholesterol transporter and is upregulated in response to endoplasmic
389 reticulum (ER) stress [48-50]. *STARD5* overexpressing cells showed downregulation of
390 various cholesterol-related gene sets such as “sterol biosynthetic process”, “sterol
391 metabolic process”, and “regulation of cholesterol biosynthesis by SREBP (SREBF)”
392 (**Figure 4D-4E**). Thirdly, *HSD17B12* encodes a steroid dehydrogenase involved in
393 converting estrone into estradiol and is essential for proper lipid homeostasis [51-53].
394 *HSD17B12* overexpressing cells showed downregulation of cholesterol-related gene
395 sets, including “sterol biosynthetic process” and “regulation of cholesterol biosynthesis
396 by SREBF (SREBP)” (**Supplementary Figure S9D-S9E**). Finally, *RNF5* encodes an
397 ER and mitochondrial-bound E3 ubiquitin-protein ligase that ubiquitin-tags proteins for
398 degradation [54-57]. *RNF5* overexpressing cells demonstrated alterations in gene sets
399 involved in proteostasis and ER biology, including upregulation of “ERAD pathway”,

400 “response to endoplasmic reticulum stress”, and “intra-Golgi and retrograde Golgi-to-ER
401 traffic” (**Supplementary Figure S9F-S9G**). These results suggest that our approach
402 leads to biological changes consistent with the known biological impact of the genes
403 being overexpressed.

404

405 Next, we sought to determine whether modulation of candidate genes had any
406 impact on TE expression in general, and L1 in particular. Although there were no
407 significant changes for individual TE subfamilies following *IL16* and *STARD5*
408 overexpression (**Supplementary Table S5A-S5B**), we identified subtle but widespread
409 upregulation of various TE families across both conditions by GSEA (**Figure 4F**,
410 **Supplementary Table S5Q-S5R**). Interestingly, 7 families, including L1, ERV1, ERVL-
411 MaLR, Alu, ERVL, TcMar-Tigger, and hAT-Charlie families, were commonly
412 upregulated under both conditions (**Figure 4F**). In contrast, cells overexpressing
413 *HSD17B12* or *RNF5* did not drive widespread changes in L1 family expression, as
414 assessed by GSEA (**Supplementary Table S5S-S5T**). Noteworthy, the L1 family gene
415 set was more strongly upregulated following *STARD5* overexpression (NES = 2.25,
416 FDR = 6.14E-7) compared to *IL16* overexpression (NES = 2.24, FDR = 2.40E-5)
417 (**Figure 4G, Supplementary Table S5Q-S5R**). Since *IL16* is upregulated in response to
418 *STARD5* overexpression, this suggests that *STARD5* may synergize with *IL16* for the
419 regulation of L1 transcription.

420

421 Then, we decided to further characterize the impact of IL16 activity on TEs, since
422 (i) its overexpression led to a global upregulation of TE transcription, and (ii) it was itself

423 upregulated in response to *STARD5* overexpression, which also led to increased TE
424 expression. Thus, since IL16 is a soluble cytokine, we independently assessed its
425 regulatory properties by exposing GM12878 cells to recombinant human IL16 peptide
426 [rhIL16] for 24 hours (**Figure 5A, Supplementary Figure S10A**). Differential gene
427 expression analysis (**Supplementary Table S6A**) and comparison with the *IL16*
428 overexpression results demonstrated that differentially expressed genes were weakly
429 but significantly correlated (**Supplementary Figure S10B**). Additionally, we carried out
430 GSEA using the GO Biological Process, Reactome pathway, and Hallmark pathway
431 gene sets (**Supplementary Table S6B-S6E**) and compared those results with the
432 GSEA from the *IL16* overexpression (**Supplementary Table S6F-S6H**). Consistent with
433 the known biology of *IL16*, GSEA highlighted a downregulation of many immune cell-
434 related gene sets, including “leukocyte differentiation”, “mononuclear cell differentiation”,
435 and “Interleukin-10 signaling” (**Figure 5B-5C, Supplementary Table S6F-S6H**). Like
436 the overexpression results, exposure of GM12878 to rhIL16 for 24 hours led to an
437 upregulation of an L1 family gene set by GSEA, although the effect was less
438 pronounced than with the overexpression (**Figure 5D**). Even though treatment of
439 GM12878 with rhIL16 for 48 hours exhibited known features of IL16 biology
440 (**Supplementary Figure S10B-S10D, Supplementary Table S6J-S6Q**), the L1
441 upregulation was no longer detectable, though other TEs remained upregulated
442 (**Supplementary Figure S10E, Supplementary Table S6Q**). These results further
443 support the notion that *IL16* acts as a modulator of L1 expression.

444

445 Finally, we sought to define the biological pathways regulated concomitantly with
446 the L1 family gene set under all experimental conditions where it was upregulated (i.e.,
447 *IL16* overexpression, *STARD5* overexpression, and 24 hours of rhIL16 exposure)
448 **(Figure 6A, Figure 6B, Supplementary Table S7A)**. Again, we reasoned that such
449 pathways would act either upstream (as regulatory pathways) or downstream (as
450 response pathways) of TE alterations. GSEA with the Hallmark pathway gene sets
451 identified 7 gene sets fitting this criterion, including “TNF α signaling via NF-KB”, “IL2
452 STAT5 signaling”, “inflammatory response”, “mTORC1 signaling”, “estrogen response
453 early”, “apoptosis”, and “UV response up” **(Figure 6C, Supplementary Table S7B)**.
454 GSEA with the GO Biological Process gene sets **(Figure 6D, Supplementary Table**
455 **S7C)** and the Reactome pathway gene sets **(Figure 6E, Supplementary Table S7D)**
456 also identified MAPK signaling, virus-related pathways like “HCMV early events”,
457 pathways involved in cell differentiation, and pathways involved in cholesterol and
458 steroid metabolism like “signaling by nuclear receptors”. These results further cement
459 the catalogue of pathways associated with differences in TE expression.

460

461

462 *L1 trans-eQTLs are co-associated with aging traits in GWAS databases.*

463 Although TE de-repression has been observed broadly with aging and age-
464 related disease [5, 58], whether this de-repression acts as a causal driver, or a
465 downstream consequence, of aging phenotypes remains unknown. We reasoned that if
466 increased TE expression at least partially drives aging phenotypes, L1 *trans*-eQTLs

467 should be enriched for associations to aging traits in genome-wide association studies
468 [GWAS] or phenome-wide association studies [PheWAS].

469

470 To test our hypothesis, we queried the Open Targets Genetics platform with our
471 499 *trans*-eQTL SNVs, mapped traits to standardized MeSH IDs, and then manually
472 curated MeSH IDs related to aging-related traits (**Figure 7A**). Consistent with our
473 hypothesis, a large proportion of L1 *trans*-eQTL SNVs (222/499 or 44.5%) were either
474 (i) associated with an aging MeSH trait by PheWAS or (ii) LD-linked to a lead variant
475 associated with an aging MeSH trait (**Figure 7B**). Moreover, among the 222 SNVs with
476 significant aging-trait associations, we observed frequent mapping to more than a single
477 age-related trait by PheWAS, with many SNVs associated with 10-25 traits (**Figure 7C**,
478 **Supplementary Table S8A**). Additionally, many of the 222 SNVs mapped to 1-5 aging
479 traits through a proxy lead variant (**Figure 7D**, **Supplementary Table S8A**). Among the
480 most frequently associated or linked traits, we identified type 2 diabetes mellitus,
481 hyperparathyroidism, thyroid diseases, coronary artery disease, hypothyroidism, and
482 psoriasis, among many others (**Figure 7E**, **Supplementary Table S8B**).

483

484 As a parallel approach, we queried the Open Targets Genetics platform with our
485 L1 *trans*-eQTL SNVs, as well as 500 combinations of random SNVs sampled from all
486 SNVs used in the eQTL analyses. We then leveraged broader phenotype categories
487 annotated by the platform, including 14 disease categories that we considered aging-
488 related, to determine whether L1 eQTL associations were enriched for any disease
489 categories (**Supplementary Figure S11A**). L1 eQTL associations were significantly

490 enriched (FDR < 0.05 and ES > 1) for 13 out of 14 disease categories, including cell
491 proliferation disorders, immune system diseases, and musculoskeletal diseases
492 **(Supplementary Figure S11B-N)**. The cardiovascular diseases category was the only
493 disease category for which we did not observe a significant enrichment
494 **(Supplementary Figure S11O)**. The enrichment for cell proliferation disorders is
495 consistent with the associations of L1 activity with cellular senescence [12, 15] and
496 cancer [59, 60]. The enrichment for immune system diseases is consistent with the role
497 of L1 as a stimulator of the interferon pathway, inflammation, and senescence [15], as
498 well as the more general notion that transposons can mimic viruses and stimulate
499 immune responses from their hosts [61]. The enrichment for musculoskeletal diseases
500 is consistent with an increase in L1 expression and copy number with age in muscle
501 tissue from aging mice [11]. These results reinforce the notion that L1 activity is strongly
502 and non-randomly associated with an assortment of age-related diseases.

503

504 Intriguingly, a large fraction of co-associated SNVs were on chromosome 6 near
505 the HLA locus, which has previously been shown to be a hotspot of age-related disease
506 traits [62]. Despite its association to our strongest L1 trans-eQTL SNV, little is known
507 about the regulation and impact of IL16 during aging. One study, however, found that
508 *IL16* expression increases with age in ovarian tissue, and the frequency of *IL16*
509 expressing cells is significantly higher in ovarian tissue from women at early and late
510 menopause, compared to premenopausal women [63]. Given these findings, and since
511 L1 expression levels and copy number have been found to increase with age [5], we
512 asked whether circulating IL16 levels may also change with age, using C57BL/6JNia

513 mice as a model (**Figure 7F, Supplementary Table S8C**). Consistent with the notion
514 that increased IL16 levels may, at least partially, drive age-related TE de-repression, we
515 observed a significant increase in circulating IL16 levels in female mice with age, and a
516 trending increase with age in male mice (although the levels showed more animal-to-
517 animal variability). By meta-analysis, circulating IL16 levels changed significantly with
518 age across sexes (**Figure 7F**). These results further support the hypothesis that *IL16* is
519 involved in L1 biology and may modulate L1 age-related changes. In sum, our results
520 provide one of the first pieces of evidence of a causal link between L1 expression levels
521 and age-related decline.

522

523

524 **DISCUSSION**

525 In this work, we developed a pipeline to computationally identify candidate L1
526 transcriptional regulators by eQTL analysis. We provide experimental evidence for the
527 involvement of top candidates in regulating L1 expression, demonstrating as a proof-of-
528 principle that this approach can be broadly used on other large “omic”-characterized
529 cohorts with human (i.e. GTEx [64, 65] or HipSci [66]) or mouse (i.e. DO mice [67])
530 subjects to identify other regulators of L1 activity. These datasets, combined with our
531 approach, could be utilized to rigorously characterize conserved or group-specific TE
532 regulatory mechanisms on multiple layers, such as across TE families (like Alu or
533 ERVs), across cell or tissue types, across ancestry groups, and across species. This
534 approach, which leverages existing datasets to perform *in silico* screening, could be a
535 powerful method to expand our knowledge of TE regulation in non-diseased cells and
536 tissues.

537
538 While we believe this approach can readily be applied to other datasets, we
539 would like to note potential limitations with the approach implemented here, some of
540 which were simply beyond the scope of this paper. Firstly, though it is common to use
541 probabilistic estimation of expression residuals (PEER) [68] to enhance detection of *cis*-
542 eQTLs, PEER was not implemented in our analysis as a precautionary measure, in
543 order to avoid potentially blurring global TE signals, which likely led to a more
544 conservative list of candidate *cis* gene mediators. Second, given the technical
545 complexity in generating the vast amount of mRNA-seq data used for the eQTL
546 analysis, it is possible that technical covariates introduced non-linear effects that would

547 not be easily removed by approaches like PEER or SVA [69]. For that reason, we opted
548 to supplement our computational predictions with experimental data. Third, the L1 *trans*-
549 eQTLs identified were specific to older L1 subfamilies (L1P and L1M) and were not
550 shared across subfamilies. One factor that may partially explain this is the heightened
551 difficulty of quantifying the expression of evolutionarily younger L1 subfamilies using
552 short-read sequencing [70]. More generally, significant single gene differences are often
553 difficult to reproduce across studies, and it is for this reason that methods like GSEA
554 were developed, to robustly identify broader changes in sets of genes [29]. Consistently,
555 GSEA suggests that many TE families, beyond the single L1 subfamilies identified in
556 the eQTL analysis, are differentially regulated among samples with different genotypes
557 for *trans*-eQTL SNVs and among samples where *IL16/IL16* and *STARD5* were
558 manipulated. We note that although *HLA* and *HSD17B12* loci were significant in both
559 the European and African cohorts, we were not able to independently identify all of the
560 same candidate regulators. This is likely due to a combination of small sample size for
561 the African cohort and the existence of population-specific L1 regulation. Future studies
562 with larger sample sizes may be useful for expanding the catalogue of loci that are
563 biologically meaningful for L1 expression across more than one population. Importantly,
564 our computational scan is limited to loci exhibiting genomic variation among tested
565 individuals. This will vary with factors like the ancestry groups of the populations being
566 studied. Moreover, variants that confer extreme fitness defects may not exist at a
567 sufficiently high level in a population so as to allow for an assessment of their
568 involvement as eQTLs. Also, a potential “blindspot” of our current approach is that it
569 does not distinguish between TE reads of intronic or intergenic origin. Intronic TE RNA

570 is often considered less interesting from a biological perspective since their presence
571 may be attributed to readthrough transcription [71]. However, all analyses carried out in
572 this study relied on polyA-selected libraries, which should be enriched for mature gene
573 and transposon transcripts, minimizing the presence of readthrough transcribed L1
574 RNA. Additionally, even if L1-containing transcripts were quantified, these have been
575 implicated in tightly controlled functions like T-cell quiescence maintenance [31],
576 suggesting that intronic L1 RNA possesses biologically meaningful properties. Thus,
577 this pipeline should help expand our understanding of L1 biology in either case. Finally,
578 although we focused on protein-coding candidate regulators, it is possible that the non-
579 coding genes identified in our scan may also causally drive differences in L1
580 expression. Though not explored here, other regulatory factors like small RNAs may
581 also act as partial mediators. Since the GEUVADIS Consortium generated small RNA
582 data in parallel to the mRNA data used in this study [26], in the future, our pipeline could
583 be adapted to scan for *cis* small RNA mediators relatively easily. These unexplored
584 factors may explain the associations between orphan SNV genotypes and TE family
585 gene set changes.

586

587 Despite potential limitations, our approach identified *IL16*, *STARD5*, *HLA-DRB5*,
588 *HLA-DQA2*, *HSD17B12*, *RNF5*, *FKBPL*, and *EHMT2-AS1* as candidate L1 regulators in
589 the European cohort. Moreover, the upregulation of several TE gene sets following
590 *IL16/IL16* and *STARD5* manipulation highlights a causal role for these genes in TE
591 control. Between these two genes, multiple lines of evidence suggest that *STARD5* is
592 the more potent mediator. First, the three-part integration statistics are more significant

593 for *STARD5* than for *IL16*. Second, the index SNV on chromosome 15 exhibited
594 significant mediation effects through *STARD5* but not *IL16*; the most significant
595 mediation effect for *IL16* was linked to a clumped SNV. Third, the upregulation for the
596 L1 family gene set was stronger under *STARD5* overexpression than under *IL16*
597 overexpression. Importantly, we observed that *IL16* was upregulated following *STARD5*
598 overexpression, but this upregulation was less than the upregulation from the *IL16*
599 overexpression. This suggests that *IL16* can participate in the L1-regulating properties
600 exerted by *STARD5*. Moving forward, it will be informative to assess the effects of *IL16*
601 and *STARD5* on L1 expression in other cell types. Interestingly, other genes like
602 *EHMT2* have previously been linked to retrotransposons [72, 73]. For the remaining
603 genes that we experimentally tested, we note that GM12878 is predicted to have
604 relatively high endogenous *HSD17B12* expression and intermediate *RNF5* expression,
605 based on the GM12878 genotypes at *cis*-eQTLs for these genes. Given these
606 expression patterns, GM12878 may not be sensitive to overexpression of *RNF5*, and
607 especially insensitive to *HSD17B12* overexpression. For these two candidates, cells
608 may be more sensitive to knockdown- or knockout-based approaches. Indeed,
609 *HSD17B12* is essential for mouse development, *HSD17B12* knockout in adult mice
610 results in reduced body weight and liver toxicity, and knockdown of the *Caenorhabditis*
611 *elegans* ortholog for *HSD17B12* reduces lipid stores and blocks induction of the
612 unfolded protein response of the endoplasmic reticulum [52, 74, 75]. Given that TEs are
613 often derepressed when homeostasis is challenged [61], such as following *HSD17B12*
614 knockout/knockdown, it remains possible that *HSD17B12* possesses L1 regulatory
615 properties that were not detectable by our approach. Future work could avert such

616 technical limitations by testing the impact of candidate genes by both up- and down-
617 regulation, or by selecting LCL samples with endogenous target gene expression levels
618 that would be most sensitive to our overexpression approach.

619

620 As another, theoretical line of evidence for the potential involvement of candidate
621 genes in L1 regulation, we highlight known interactions between tested candidate genes
622 and viral infections, which may be relevant under conditions where transposons are
623 recognized as viral mimics [61]. Indeed, *IL16* has been extensively studied for its ability
624 to inhibit human immunodeficiency virus (HIV) replication, partly by suppressing mRNA
625 expression [76-78]. Additionally, but in contrast to its HIV-suppressive properties, *IL16*
626 can enhance the replication of influenza A virus (IAV) and facilitate its infection of hosts,
627 potentially through its repression of type I interferon beta and interferon-stimulated
628 genes [79]. *IL16* can also contribute to the establishment of lifelong gamma herpesvirus
629 infection [80]. *STARD5* is another candidate implicated in the influenza virus replication
630 cycle [81]. *HSD17B12* promotes the replication of hepatitis C virus via the very-long-
631 chain fatty acid (VLCFA) synthesis pathway and the production of lipid droplets
632 important for virus assembly [82, 83]. Additionally, HSD17B12 has been found
633 interacting with the coronavirus disease 2019 (COVID-19) protein nonstructural protein
634 13 (NSP13), which is thought to antagonize interferon signaling [84]. Finally, *RNF5* has
635 been implicated in both promoting and antagonizing severe acute respiratory syndrome
636 coronavirus 2 (SARS-CoV-2) by either stabilizing the interactions of membrane protein
637 (M) [85] or inducing degradation of structural protein envelope (E) [86], respectively.
638 Fundamentally, *RNF5* regulates virus-triggered interferon signaling by targeting the

639 stimulator of interferon genes (STING) or mitochondrial antiviral signaling protein
640 (MAVS) for ubiquitin-mediated protein degradation [56, 57]. These studies reinforce the
641 roles of tested candidate regulators in virus-associated processes, including interferon-
642 mediated signaling.

643

644 Consistent with the notion that L1 is associated with aging and aging phenotypes
645 [5, 58], we observed that L1 *trans*-eQTL SNVs were associated with aging phenotypes
646 in GWAS/PheWAS databases. This is very surprising, but interesting, given that all
647 1000Genomes Project participants declared themselves to be healthy at the time of
648 sample collection. Assuming this to be true, our results suggest that L1 expression
649 differences exist in natural, healthy human populations, and these expression
650 differences precede onset of aging diseases. Though it is often unclear whether L1 mis-
651 regulation is a consequence or driver of aging phenotypes, our results suggest that L1
652 levels may drive aging phenotypes. As we continue to expand the catalogue of L1
653 regulators, especially in healthy cells and tissues, the L1 regulatory processes that are
654 disrupted over the course of aging will become increasingly clear. To that end, this work
655 may serve as a guide for conducting more comprehensive scans for candidate TE
656 regulators.

657

658

659 CONCLUSIONS

660 We developed an eQTL-based pipeline that leverages genomic and
661 transcriptomic data to scan the human genome for novel candidate regulators of L1
662 subfamily expression. Though the initial scan identified genetic variants associated with
663 expression differences in specific L1 subfamilies, secondary analyses by GSEA suggest
664 that genetic variants are associated with subtle but global differences in the expression
665 of many TE families. Our pipeline identified candidate genes, including *HSD17B12* and
666 *HLA* genes, that likely play a conserved role in L1 regulation across human populations
667 of different ancestries. Though some top candidates from the European cohort scan,
668 such as *IL16*, *STARD5*, and *RNF5*, were not significant in the African cohort analysis, it
669 is likely that some of these genes would appear in cross-ancestry scans with larger
670 samples sizes. We detected subtle but global differences in L1 family expression
671 following *IL16* overexpression, *STARD5* overexpression, and rhIL16 treatment for 24
672 hours, further suggesting that some candidate genes have regulatory potential. We
673 generate a list of pathways, such as mTORC1 signaling and cholesterol metabolism,
674 that may act upstream of L1 expression. Finally, the co-association of some genetic
675 variants with both L1 expression differences and various age-related diseases suggests
676 that L1 differences may precede and contribute to the onset of disease. Our results
677 expand the potential mechanisms by which L1 expression is regulated and by which L1
678 may influence aging-related phenotypes.

679

680

681 **METHODS**

682 **Publicly available data acquisition**

683 The eQTL analysis was carried out on 358 European (EUR) individuals and 86
684 Yoruban (YRI) individuals for which paired single nucleotide variant, structural variant,
685 and transcriptomic data were available from Phase 3 of the 1000 Genomes Project [22,
686 23] and from the GEUVADIS consortium [26]. Specifically, Phase 3 autosomal SNVs
687 called on the GRCh38 reference genome were obtained from The International Genome
688 Sample Resource (IGSR) FTP site (
689 [http://ftp.1000genomes.ebi.ac.uk/vol1/ftp/data_collections/1000_genomes_project/relea](http://ftp.1000genomes.ebi.ac.uk/vol1/ftp/data_collections/1000_genomes_project/release/20190312_biallelic_SNV_and_INDEL/)
690 [se/20190312_biallelic_SNV_and_INDEL/](http://ftp.1000genomes.ebi.ac.uk/vol1/ftp/data_collections/1000_genomes_project/release/20190312_biallelic_SNV_and_INDEL/)). Structural variants were also obtained from
691 the IGSR FTP site
692 (http://ftp.1000genomes.ebi.ac.uk/vol1/ftp/phase3/integrated_sv_map/). mRNA-
693 sequencing fastq files generated by the GEUVADIS consortium were obtained from
694 ArrayExpress under accession E-GEUV-1.

695

696

697 **Aggregating and pre-processing genotype data for eQTL analyses**

698 To prepare SNVs for association analyses, all SNVs were first annotated with
699 rsIDs from dbSNP build 155 using BCFtools v1.10.2 [87]. VCFtools v0.1.17 [88] was
700 then used to remove indels and keep variants with the following properties in each of
701 the two populations: possessed a minimum and maximum of two alleles, possessed a
702 minor allele frequency (MAF) of at least 1%, passed Hardy-Weinberg equilibrium
703 thresholding at $p < 1e-6$, with no missing samples, and located on an autosome. We

704 note here that sex chromosomes were not included in the analysis since (i) Y
705 chromosome SNVs were not available and (ii) analyses with X chromosome SNVs
706 require unique algorithms and cannot simply be incorporated into traditional association
707 pipelines [89, 90]. VCF files containing these filtered SNVs were then converted to
708 PLINK BED format using PLINK v1.90b6.17 [91], keeping the allele order. PLINK BED
709 files were subsequently used to generate preliminary 0/1/2 genotype matrices using the
710 '--recodeA' flag in PLINK. These preliminary matrices were manipulated in terminal,
711 using the gcut v9.0 function to remove unnecessary columns and datamash v1.7 to
712 transpose the data, to generate the final 0/1/2 matrices used for the eQTL analyses.
713 Finally, PLINK was used to prune the list of filtered SNVs, using the "--indep-pairwise 50
714 10 0.1" flag, and to generate principal components (PCs) from the pruned genotypes.

715

716 To control for inter-individual differences in genomic transposon copy number
717 load, we applied 1 of 2 approaches, depending on the analysis. For approach 1, the net
718 number of L1 and Alu insertions was quantified across the 444 samples. We chose to
719 aggregate the L1 and Alu copy numbers, since Alu relies on L1 machinery for
720 mobilization [92], and so the aggregate number may provide a finer view of L1-
721 associated copy number load. Briefly, VCFTools was used to extract autosomal
722 structural variants from the 1000Genomes structural variant calls. L1 and Alu insertions
723 and deletions were then extracted with BCFtools by keeping entries with the following
724 expressions: 'SVTYPE="LINE1"', 'SVTYPE="ALU"', 'SVTYPE="DEL_LINE1"', and
725 'SVTYPE="DEL_ALU"'. The resulting VCF files were then transformed to 0/1/2 matrices
726 in the same manner as the SNVs. A net copy number score was obtained for each

727 sample by adding the values for the L1 and Alu insertions and subtracting the values for
728 the L1 and Alu deletions. For approach 2, the complete structural variant matrix was
729 filtered with VCFtools using the same parameters as with the SNV matrices. The filtered
730 structural variant matrix was then pruned with PLINK, and these pruned structural
731 variant genotypes were used to generate principal components, in the same fashion as
732 with the SNV matrix. The net copy number score or the structural variant principal
733 components, depending on the analysis, were included as covariates.

734

735

736 **mRNA-seq read trimming, mapping, and quantification**

737 Fastq files were first trimmed using fastp v0.20.1 [93] with the following
738 parameters: detect_adapter_for_pe, disable_quality_filtering, trim_front1 17, trim_front2
739 17, cut_front, cut_front_window_size 1, cut_front_mean_quality 20, cut_tail,
740 cut_tail_window_size 1, cut_tail_mean_quality 20, cut_right, cut_right_window_size 5,
741 cut_right_mean_quality 20, and length_required 36. Read quality was then inspected
742 using fastqc v0.11.9.

743

744 Next, the GRCh38 primary human genome assembly and comprehensive gene
745 annotation were obtained from GENCODE release 33 [94]. Since LCLs are generated
746 by infecting B-cells with Epstein-Barr virus, the EBV genome (GenBank ID V01555.2)
747 was included as an additional contig in the human reference genome. The trimmed
748 reads were aligned to this modified reference genome using STAR v2.7.3a [95] with the
749 following parameters: outFilterMultimapNmax 100, winAnchorMultimapNmax 100, and

750 outFilterMismatchNoverLmax 0.04. Finally, the TEcount function in the Tetranscripts
751 v2.1.4 [27] package was employed to obtain gene and TE counts, using the GENCODE
752 annotations to define gene boundaries and a repeat GTF file provided on the Hammell
753 lab website (downloaded on February 19 2020 from
754 [https://labshare.cshl.edu/shares/mhammelllab/www-](https://labshare.cshl.edu/shares/mhammelllab/www-data/Tetranscripts/TE_GTF/GRCh38_GENCODE_rmsk_TE.gtf.gz)
755 [data/Tetranscripts/TE_GTF/GRCh38_GENCODE_rmsk_TE.gtf.gz](https://labshare.cshl.edu/shares/mhammelllab/www-data/Tetranscripts/TE_GTF/GRCh38_GENCODE_rmsk_TE.gtf.gz)) to define repeat
756 boundaries.

757

758

759 **Gene *cis*-eQTL and L1 *trans*-eQTL analyses**

760 Gene and TE count files were loaded into R v4.2.1. Lowly expressed genes were
761 first filtered out if 323/358 European samples and 78/86 Yoruban samples did not have
762 over 0.44 counts per million (cpm) or 0.43 cpm, respectively. These fractions were
763 selected because they corresponded to expression in ~90% of samples and thus helped
764 maintain maximal statistical power by focusing on genes ubiquitously expressed across
765 each entire population. The cpm thresholds were selected because they corresponded
766 to 10 reads in the median-length library within each set of samples.

767

768 Then, counts underwent a variance stabilizing transformation (vst) using DESeq2
769 v1.36.0 [96]. The following covariates were regressed out from vst normalized
770 expression data using the 'removeBatchEffect' function in Limma v3.52.2 [97]: lab,
771 population category, principal components 1-2 of the pruned SNVs, biological sex, net
772 L1/Alu copy number, and EBV expression levels. Since the Yoruban samples were all

773 from the same population, the population variable was omitted in their batch correction.
774 Here, we note several things. First, EBV expression was included as a covariate
775 because heightened TE expression is often a feature of viral infections [98]. Secondly,
776 although PEER [68] is often used to remove technical variation for *cis*-eQTL analysis,
777 this can come at the expense of correcting out genome-wide biological effects. This can
778 be problematic in some settings, such as *trans*-eQTL analysis. Thus, PEER factors
779 were not included. The batch-corrected data underwent a final inverse normal
780 transformation (INT), using the RankNorm function in the R package RNOmni v1.0.1, to
781 obtain normally distributed gene expression values.

782

783 The INT expression matrices were split into genes and L1 subfamilies, which
784 were used to identify gene *cis*-eQTLs and L1 subfamily *trans*-eQTLs in the European
785 superpopulation using MatrixEQTL v2.3 [99]. For gene *cis*-eQTLs, SNVs were tested for
786 association with expressed genes within 1 million base pairs. We opted to use a *trans*-
787 eQTL approach using aggregate subfamily-level TE expression since the *trans*
788 approach should allow us to identify regulators of many elements rather than one. The
789 Benjamini-Hochberg false discovery rate (FDR) was calculated in each analysis, and we
790 used the p-value corresponding to an FDR of < 5% as the threshold for eQTL
791 significance. In addition, the *cis*-eQTL and *trans*-eQTL analyses were also repeated
792 using 20 permuted expression datasets in which the sample names were scrambled,
793 and the p-value corresponding to an average empirical FDR of < 5% was used as a
794 secondary threshold. To note, we calculated the average empirical FDR at a given p-
795 value p_i by (i) counting the total number of null points with $p \leq p_i$, (ii) dividing by the

796 number of permutations, to obtain an average number of null points with $p \leq p_i$, and (iii)
797 dividing the average number of null points with $p \leq p_i$ by the number of real points with p
798 $\leq p_i$. eQTLs were called as significant if they passed the stricter of the two thresholds.
799 SNV-gene and SNV-L1 associations that were significant in the European
800 superpopulation were then targeted and tested in the Yoruban population using R's
801 built-in linear modelling functions. In this case, only the Benjamini-Hochberg FDR was
802 calculated, and significant eQTLs were called if they possessed an FDR < 5%.

803

804

805 **Defining SNV-gene-L1 trios and mediation analysis**

806 For each population, the *cis*- and *trans*-eQTL results were integrated to identify
807 SNVs associated with both gene and L1 subfamily expression. We reasoned that L1
808 expression would respond to differences in expression of *bona fide* regulators.
809 Consequently, gene expression and L1 subfamily expression associations were
810 assessed by linear regression, and the p-values from this analysis were Benjamini-
811 Hochberg FDR-corrected. Candidate SNV-gene-L1 trios were defined as those with *cis*-
812 eQTL, *trans*-eQTL, and expression regression FDRs < 5%. To identify top, index SNVs
813 in regions of linkage disequilibrium (LD), SNVs within 500 kilobases of each other with
814 an $R^2 > 0.10$ were clumped together by *trans*-eQTL p-value using PLINK v1.90b6.17.
815 Mediation analysis was carried out using the 'gmap.gpd' function in eQTLMAPT v0.1.0
816 [100] on all candidate SNV-gene-L1 trios. Empirical p-values were calculated using
817 30,000 permutations, and Benjamini-Hochberg FDR values were calculated from

818 empirical p-values. Mediation effects were considered significant for trios with FDR <
819 5%.

820

821

822 **Differential expression analysis across *trans*-eQTL SNV genotypes**

823 Transcriptomic changes associated with alternating the allele of each SNV of
824 interest were evaluated using DESeq2 v1.36.0. Using the same filtered counts prepared
825 for the eQTL analysis, a linear model was constructed with the following covariates for
826 each SNV: SNV genotype in 0/1/2 format, biological sex, lab, population category,
827 principal components 1-2 of the pruned SNVs, and principal components 1-3 of the
828 pruned SVs (to account for structural variant population structure). As before, the
829 population label was omitted from the Yoruban population analysis. Significant genes
830 and TEs were those with an FDR < 5%.

831

832

833 **Functional enrichment analyses**

834 We used the Gene Set Enrichment Analysis (GSEA) paradigm as implemented
835 in the R package clusterProfiler v4.4.4 [101]. Gene Ontology, Reactome, and Hallmark
836 pathway gene sets were obtained from the R package msigdb v7.5.1, an Ensembl ID-
837 mapped collection of gene sets from the Molecular Signature Database [29, 30].
838 Additionally, TE subfamilies were aggregated into TE family gene sets using the TE
839 family designations specified in the TE GTF file (downloaded on February 19 2020 from
840 [38](https://labshare.cshl.edu/shares/mhammelllab/www-</p></div><div data-bbox=)

841 data/TEtranscripts/TE_GTF/GRCh38_GENCODE_rmsk_TE.gtf.gz) used during the
842 RNA-seq quantification step. The DESeq2 v1.36.0 Wald-statistic was used to generate
843 a combined ranked list of genes and TEs for functional enrichment analysis. All gene
844 sets with an FDR < 5% were considered significant. For plots with a single analysis, the
845 top 5 downregulated and top 5 upregulated gene sets were plotted, at most. For plots
846 with multiple analyses, shared gene sets with the desired expression patterns in each
847 individual analysis were first identified. Then, the p-values for shared gene sets were
848 combined using Fisher's method, and this meta-analysis p-value was used to rank
849 shared gene sets. Finally, the top 5 gene sets with one expression pattern and the top 5
850 gene sets with the opposite expression pattern were plotted. If there were less than 5
851 gene sets in either group, those were replaced with gene sets exhibiting the opposite
852 regulation, in order to plot 10 shared gene sets whenever possible.

853

854

855 **Cell lines and cell culture conditions.**

856 GM12878 (RRID: CVCL_7526) lymphoblastoid cells were purchased from the
857 Coriell Institute. We opted to use GM12878 as a well-characterized representative cell
858 line for candidate validation, given that (i) it is of the same cell type as the transcriptomic
859 data used here for our eQTL analysis, and (ii) its epigenomic landscape and culture
860 conditions are well-characterized as part of the ENCODE project [39, 40].

861

862 GM12878 cells were maintained in RPMI (Corning cat. 15-040-CV) containing
863 15% FBS and 1X Penicillin-Streptomycin-Glutamine (Corning cat. 30-009-CI). Cells

864 were cultured in a humidified incubator at 37°C and 5% CO₂, subculturing cells 1:5 once
865 cells reached a density of ~10⁶ mL⁻¹. All cells used were maintained below passage 30
866 and routinely tested for mycoplasma contamination using the Plasmotest Mycoplasma
867 Detection Kit (InvivoGen).

868

869

870 **Plasmids**

871 The empty pcDNA3.1(+) backbone (Invitrogen cat. V79020) was a kind gift from
872 the lab of Dr. Changhan David Lee at the University of Southern California Leonard
873 Davis School of Gerontology. Overexpression vectors for *IL16* (CloneID OHu48263C),
874 *STARD5-FLAG* (CloneID OHu07617D), *HSD17B12-FLAG* (CloneID OHu29918D), and
875 *RNF5-FLAG* (CloneID OHu14875D) on a pcDNA3.1 backbone were purchased from
876 GenScript. Plasmid sequences were verified for accuracy using Plasmidsaurus's whole
877 plasmid sequencing service.

878

879

880 **Transfections**

881 *Escherichia coli* were cultured in LB Broth (ThermoFischer Scientific)
882 supplemented with 50 µg/mL carbenicillin to an optical density 600 (OD₆₀₀) of 2 – 4.
883 Plasmid extractions were carried out using the Nucleobond Xtra Midi Plus EF kit
884 (Macherey-Nagel) following manufacturer recommendations. Plasmids were aliquoted
885 and stored at -20°C until the time of transfection. On the day of transfection, GM12878
886 cells were collected in conical tubes, spun down (100xG, 5 minutes, room temperature),

887 resuspended in fresh media, and counted by trypan blue staining using a Countess II FL
888 automated cell counter (Thermo Fisher). The number of cells necessary for the
889 experiment were then aliquoted, spun down, and washed with Dulbecco's phosphate-
890 buffered saline (DPBS)(Corning, cat. #21-031-CV).

891

892 GM12878 cells were transfected by electroporation using the Neon Transfection
893 System (Invitrogen) with the following parameters: 1200 V, 20 ms, and 3 pulses for
894 GM12878 cells in Buffer R. Per reaction, we maintained a plasmid mass:cell number
895 ratio of 10 μg : 2×10^6 cells. For mRNA-sequencing, 8×10^6 GM12878 cells were
896 independently transfected for each biological replicate, with 4 replicates per
897 overexpression condition, and cultured in a T25 flask. Immediately after transfection,
898 cells were cultured in Penicillin-Streptomycin-free media for ~24 hours.

899

900 Afterwards, to promote selection of viable and healthy transfected GM12878
901 cells, we enriched for viable cells using the EasySep Dead Cell Removal (Annexin V)
902 Kit (STEMCELL Technologies) before seeding 2×10^6 live cells in the same media used
903 for cell maintenance. After another 24 hours, cell viability was measured by trypan blue
904 staining on a Countess automated cell counter and cells were spun down (100xG, 5
905 min, room temperature) and lysed in TRIzol Reagent (Invitrogen) for downstream total
906 RNA isolation (see below).

907

908

909 **Recombinant human IL16 (rhIL16) peptide treatment**

910 Human rhIL16 was obtained from PeproTech (cat. #200-16) and resuspended in
911 0.1% bovine serum albumin (BSA) solution (Akron, cat. #AK8917-0100). GM12878 cells
912 were seeded at a concentration of 500,000 live cells per mL of media on 6-well
913 suspension plates with 3 independent replicates per condition. Cells were exposed to 0,
914 24, or 48 hours of 100 ng mL⁻¹ of rhIL16. To replace or exchange media 24 hours after
915 seeding, cells were transferred to conical tubes, spun down (100xG, 5 min, room
916 temperature), resuspended in 5 mL of the appropriate media, and transferred back to 6-
917 well suspension plates. After 48 hours, cell viability was measured by trypan blue
918 staining and cells were spun down (100xG, 5 min, room temperature) and lysed in
919 TRIzol Reagent (Invitrogen).

920

921

922 **RNA extractions and mRNA sequencing**

923 RNA was extracted using the Direct-zol RNA Miniprep kit (Zymo Research)
924 following manufacturer recommendations. The integrity of RNA samples was evaluated
925 using an Agilent High Sensitivity RNA ScreenTape assay (Agilent Technologies),
926 ensuring that all samples had a minimum eRIN score of 8 before downstream
927 processing. We then submitted total RNA samples to Novogene (Sacramento,
928 California) for mRNA library preparation and sequencing on the NovaSeq 6000 platform
929 as paired-end 150 bp reads.

930

931

932 **Analysis of overexpression and rhIL16 exposure mRNA-seq**

933 mRNA-seq reads were trimmed, mapped, and quantified like for the eQTL
934 analysis, except for the overexpression sample data. For this data, one modification
935 was made: the EBV-inclusive reference genome was further modified to include the
936 pcDNA3.1 sequence as an additional contig. Lowly expressed genes were filtered using
937 a cpm threshold as in the eQTL processing, but that cpm threshold had to be satisfied
938 by as many samples as the size of the smallest biological group. For the overexpression
939 data, surrogate variables were estimated with the 'svaseq' function [69] in the R
940 package 'sva' v3.44.9, and they were regressed out from the raw read counts using the
941 'removeBatchEffect' function in the R package Limma v3.52.2. DESeq2 was used to
942 identify significantly (FDR < 5%) differentially expressed genes and TEs between
943 groups. Functional enrichment analysis was carried out as previously described.

944

945

946 **PheWAS analysis**

947 To gather the known associated traits for the 499 TE-related SNVs, we used
948 Open Targets Genetics (<https://genetics.opentargets.org/>), a database of GWAS
949 summary statistics [102]. First, we queried the database using the 499 TE-related SNVs
950 and collected traits that were directly associated (with $P < 5 \times 10^{-8}$) with the SNVs, as well
951 as traits associated with lead variants that were in linkage disequilibrium (LD) with the
952 queried SNPs (with $R^2 > 0.6$). For age-related traits (ARTs), we used the
953 comprehensive list of 365 Medical Subject Headings (MeSH) terms reported by [103]
954 (downloaded from <https://github.com/kisudsoe/Age-related-traits>). To identify known
955 age-related traits, the known associated traits were translated into the equivalent MeSH

956 terms using the method described by [103]. Then, the MeSH-translated known
957 associated traits for the 499 TE-related SNVs were filtered by the MeSH terms for age-
958 related traits.

959

960 As a parallel approach, we mapped the RsIDs for all SNVs used during the eQTL
961 analyses to their corresponding bi-allelic Open Targets variant IDs, when available. The
962 variant IDs corresponding to L1 *trans*-eQTL SNVs were extracted, and 500 different
963 equal-length combinations of random SNVs were generated. Next, we queried the Open
964 Targets database using the lists of L1-associated and random SNVs and collected the
965 associated traits (with $P < 5 \times 10^{-8}$). Importantly, the database assigns traits to broader
966 categories, including 14 disease categories that we considered age-related. We
967 counted the number of L1-associated or random SNVs mapping to each category, and
968 we used the random SNV counts to generate an empirical cumulative distribution
969 function (ecdf) for each category. We calculated enrichment p-values using the formula
970 $p = 1 - \text{ecdf}(\text{mapped eQTLs})$ and then Benjamini-Hochberg FDR-corrected all p-values.
971 An enrichment score (ES) was also calculated for each category using the formula $\text{ES} =$
972 $\text{number of mapped L1 eQTLs} / \text{median number of randomly mapping SNVs}$. Categories
973 with an $\text{ES} > 1$ and $\text{FDR} < 0.05$ were considered significantly enriched.

974

975

976 **Quantification of mouse serum IL16 by ELISA**

977 Serum was collected from male and female C57BL/6JNia mice (4-6 and 20-24
978 months old) obtained from the National Institute on Aging (NIA) colony at Charles

979 Rivers. All animals were euthanized between 8-11 am in a “snaking order” across all
980 groups to minimize batch-processing confounds due to circadian processes. All animals
981 were euthanized by CO₂ asphyxiation followed by cervical dislocation. Circulating IL16
982 levels were quantitatively evaluated from mouse serum by enzyme-linked
983 immunosorbent assay (ELISA). Serum was diluted 1/10 before quantifying IL16
984 concentrations using Abcam’s Mouse IL-16 ELISA Kit (ab201282) in accordance with
985 manufacturer instructions. Technical replicates from the same sample were averaged to
986 one value before statistical analysis and plotting. P-values across age within each sex
987 were calculated using a non-parametric 2-sided Wilcoxon test, and p-values from each
988 sex-specific analysis were combined using Fisher’s method.

989

990

991

992 **DECLARATIONS**

993

994 **Ethics approval and consent to participate**

995 All animals were treated and housed in accordance with the Guide for Care and
996 Use of Laboratory Animals. All experimental procedures were approved by the
997 University of Southern California's Institutional Animal Care and Use Committee
998 (IACUC) and are in accordance with institutional and national guidelines. Samples were
999 derived from animals on approved IACUC protocol #20770.

1000

1001 **Availability of data and materials**

1002 Sequencing data generated in this study is accessible through the Sequence
1003 Read Archive (SRA) under BioProject PRJNA937306. All code is available on the
1004 Benayoun lab GitHub (https://github.com/BenayounLaboratory/TE-eQTL_LCLs).
1005 Analyses were conducted using R version 4.2.1. Code was re-run independently on R
1006 version 4.3.0 to check for reproducibility.

1007

1008 **Competing interests**

1009 The authors declare that they have no competing interests.

1010

1011 **Funding**

1012 This material is based upon work supported by the National Science Foundation
1013 Graduate Research Fellowship Program (NSF GRFP) under Grant No. DGE-1842487
1014 (to J.I.B.), the National Institute on Aging (NIA) under Grant No. T32 AG052374 (to

1015 J.I.B.), the University of Southern California with a Provost Fellowship (to J.I.B.), the
1016 USC Gerontology Enriching MSTEM (GEMSTEM) to Enhance Diversity in Aging
1017 Program under Grant No. R25 AG076400 (to C.R.M.), and the National Institute of
1018 General Medical Sciences (NIGMS) under Grant No. R35 GM142395 (to B.A.B).

1019

1020

1021 **Authors' contributions**

1022 J.I.B. and B.A.B designed the study. J.I.B., L.Z., and S.K. performed data
1023 analyses, with guidance from Y.S. and B.A.B. J.I.B. and C.R.M. carried out
1024 experiments. J.I.B., B.A.B., S.K., and Y.S. wrote the manuscript. All authors contributed
1025 to the editing of the manuscript.

1026

1027

1028 **Acknowledgements**

1029 We would like to thank Prof. Rachel Brem for her feedback and insights on the
1030 eQTL analyses. We would also like to thank Dr. Minhoo Kim for her feedback on the
1031 manuscript. Some panels were created with BioRender.com.

1032

1033

1034

1035 **REFERENCES**

- 1036 1. Lander ES, Linton LM, Birren B, Nusbaum C, Zody MC, Baldwin J, Devon K, Dewar K,
1037 Doyle M, FitzHugh W, et al: **Initial sequencing and analysis of the human genome.**
1038 *Nature* 2001, **409**:860-921.
- 1039 2. Venter JC, Adams MD, Myers EW, Li PW, Mural RJ, Sutton GG, Smith HO, Yandell M,
1040 Evans CA, Holt RA, et al: **The Sequence of the Human Genome.** *Science* 2001,
1041 **291**:1304-1351.
- 1042 3. Brouha B, Schustak J, Badge RM, Lutz-Prigge S, Farley AH, Moran JV, Kazazian HH:
1043 **Hot L1s account for the bulk of retrotransposition in the human population.**
1044 *Proceedings of the National Academy of Sciences* 2003, **100**:5280-5285.
- 1045 4. Moran JV, Holmes SE, Naas TP, DeBerardinis RJ, Boeke JD, Kazazian HH, Jr.: **High**
1046 **Frequency Retrotransposition in Cultured Mammalian Cells.** *Cell* 1996, **87**:917-927.
- 1047 5. Bravo JI, Nozownik S, Danthi PS, Benayoun BA: **Transposable elements, circular**
1048 **RNAs and mitochondrial transcription in age-related genomic regulation.**
1049 *Development* 2020, **147**.
- 1050 6. Della Valle F, Reddy P, Yamamoto M, Liu P, Saera-Vila A, Bensaddek D, Zhang H,
1051 Prieto Martinez J, Abassi L, Celii M, et al: **LINE-1 RNA causes heterochromatin**
1052 **erosion and is a target for amelioration of senescent phenotypes in progeroid**
1053 **syndromes.** *Science Translational Medicine* 2022, **14**:eabl6057.
- 1054 7. Simon M, Van Meter M, Ablava J, Ke Z, Gonzalez RS, Taguchi T, De Cecco M,
1055 Leonova KI, Kogan V, Helfand SL, et al: **LINE1 Derepression in Aged Wild-Type and**
1056 **SIRT6-Deficient Mice Drives Inflammation.** *Cell Metabolism* 2019, **29**:871-885.e875.
- 1057 8. Zhao Y, Oreskovic E, Zhang Q, Lu Q, Gilman A, Lin YS, He J, Zheng Z, Lu JY, Lee J, et
1058 al: **Transposon-triggered innate immune response confers cancer resistance to**
1059 **the blind mole rat.** *Nature Immunology* 2021, **22**:1219-1230.

- 1060 9. Zhao H, Ji Q, Wu Z, Wang S, Ren J, Yan K, Wang Z, Hu J, Chu Q, Hu H, et al:
1061 **Destabilizing heterochromatin by APOE mediates senescence.** *Nature Aging* 2022,
1062 **2:303-316.**
- 1063 10. Liu EY, Russ J, Cali CP, Phan JM, Amlie-Wolf A, Lee EB: **Loss of Nuclear TDP-43 Is**
1064 **Associated with Decondensation of LINE Retrotransposons.** *Cell Reports* 2019,
1065 **27:1409-1421.e1406.**
- 1066 11. De Cecco M, Criscione SW, Peterson AL, Neretti N, Sedivy JM, Kreiling JA:
1067 **Transposable elements become active and mobile in the genomes of aging**
1068 **mammalian somatic tissues.** *Aging (Albany NY)* 2013, **5:867-883.**
- 1069 12. De Cecco M, Criscione SW, Peckham EJ, Hillenmeyer S, Hamm EA, Manivannan J,
1070 Peterson AL, Kreiling JA, Neretti N, Sedivy JM: **Genomes of replicatively senescent**
1071 **cells undergo global epigenetic changes leading to gene silencing and activation**
1072 **of transposable elements.** *Aging Cell* 2013, **12:247-256.**
- 1073 13. Campisi J: **Aging, Cellular Senescence, and Cancer.** *Annual Review of Physiology*
1074 2013, **75:685-705.**
- 1075 14. Franceschi C, Garagnani P, Parini P, Giuliani C, Santoro A: **Inflammaging: a new**
1076 **immune–metabolic viewpoint for age-related diseases.** *Nature Reviews*
1077 *Endocrinology* 2018, **14:576-590.**
- 1078 15. De Cecco M, Ito T, Petrashen AP, Elias AE, Skvir NJ, Criscione SW, Caligiana A,
1079 Broccoli G, Adney EM, Boeke JD, et al: **L1 drives IFN in senescent cells and**
1080 **promotes age-associated inflammation.** *Nature* 2019, **566:73-78.**
- 1081 16. Rodriguez-Martin B, Alvarez EG, Baez-Ortega A, Zamora J, Supek F, Demeulemeester
1082 J, Santamarina M, Ju YS, Temes J, Garcia-Souto D, et al: **Pan-cancer analysis of**
1083 **whole genomes identifies driver rearrangements promoted by LINE-1**
1084 **retrotransposition.** *Nature Genetics* 2020, **52:306-319.**

- 1085 17. Flasch DA, Chen X, Ju B, Li X, Dalton J, Mulder HL, Easton J, Wang L, Baker SJ,
1086 Chiang J, Zhang J: **Somatic LINE-1 promoter acquisition drives oncogenic FOXR2**
1087 **activation in pediatric brain tumor.** *Acta Neuropathologica* 2022, **143**:605-607.
- 1088 18. Levin HL, Moran JV: **Dynamic interactions between transposable elements and**
1089 **their hosts.** *Nature Reviews Genetics* 2011, **12**:615-627.
- 1090 19. Rebollo R, Romanish MT, Mager DL: **Transposable Elements: An Abundant and**
1091 **Natural Source of Regulatory Sequences for Host Genes.** *Annual Review of*
1092 *Genetics* 2012, **46**:21-42.
- 1093 20. Liu N, Lee CH, Swigut T, Grow E, Gu B, Bassik MC, Wysocka J: **Selective silencing of**
1094 **euchromatic L1s revealed by genome-wide screens for L1 regulators.** *Nature* 2018,
1095 **553**:228-232.
- 1096 21. Chung N, Jonaid GM, Quinton S, Ross A, Sexton CE, Alberto A, Clymer C, Churchill D,
1097 Navarro Leija O, Han MV: **Transcriptome analyses of tumor-adjacent somatic**
1098 **tissues reveal genes co-expressed with transposable elements.** *Mobile DNA* 2019,
1099 **10**:39.
- 1100 22. Auton A, Abecasis GR, Altshuler DM, Durbin RM, Abecasis GR, Bentley DR, Chakravarti
1101 A, Clark AG, Donnelly P, Eichler EE, et al: **A global reference for human genetic**
1102 **variation.** *Nature* 2015, **526**:68-74.
- 1103 23. Sudmant PH, Rausch T, Gardner EJ, Handsaker RE, Abyzov A, Huddleston J, Zhang Y,
1104 Ye K, Jun G, Hsi-Yang Fritz M, et al: **An integrated map of structural variation in**
1105 **2,504 human genomes.** *Nature* 2015, **526**:75-81.
- 1106 24. Sie L, Loong S, Tan EK: **Utility of lymphoblastoid cell lines.** *Journal of Neuroscience*
1107 *Research* 2009, **87**:1953-1959.
- 1108 25. Hussain T, Mulherkar R: **Lymphoblastoid Cell lines: a Continuous in Vitro Source of**
1109 **Cells to Study Carcinogen Sensitivity and DNA Repair.** *Int J Mol Cell Med* 2012,
1110 **1**:75-87.

- 1111 26. Lappalainen T, Sammeth M, Friedländer MR, 't Hoen PAC, Monlong J, Rivas MA,
1112 González-Porta M, Kurbatova N, Griebel T, Ferreira PG, et al: **Transcriptome and**
1113 **genome sequencing uncovers functional variation in humans.** *Nature* 2013,
1114 **501:506-511.**
- 1115 27. Jin Y, Tam OH, Paniagua E, Hammell M: **TEtranscripts: a package for including**
1116 **transposable elements in differential expression analysis of RNA-seq datasets.**
1117 *Bioinformatics* 2015, **31:3593-3599.**
- 1118 28. Williams TM: **Human Leukocyte Antigen Gene Polymorphism and the**
1119 **Histocompatibility Laboratory.** *The Journal of Molecular Diagnostics* 2001, **3:98-104.**
- 1120 29. Subramanian A, Tamayo P, Mootha VK, Mukherjee S, Ebert BL, Gillette MA, Paulovich
1121 A, Pomeroy SL, Golub TR, Lander ES, Mesirov JP: **Gene set enrichment analysis: A**
1122 **knowledge-based approach for interpreting genome-wide expression profiles.**
1123 *Proceedings of the National Academy of Sciences* 2005, **102:15545-15550.**
- 1124 30. Liberzon A, Birger C, Thorvaldsdóttir H, Ghandi M, Mesirov JP, Tamayo P: **The**
1125 **Molecular Signatures Database (MSigDB) hallmark gene set collection.** *Cell Syst*
1126 2015, **1:417-425.**
- 1127 31. Marasca F, Sinha S, Vadalà R, Polimeni B, Ranzani V, Paraboschi EM, Burattin FV,
1128 Ghilotti M, Crosti M, Negri ML, et al: **LINE1 are spliced in non-canonical transcript**
1129 **variants to regulate T cell quiescence and exhaustion.** *Nature Genetics* 2022,
1130 **54:180-193.**
- 1131 32. Wahl D, Cavalier AN, Smith M, Seals DR, LaRocca TJ: **Healthy Aging Interventions**
1132 **Reduce Repetitive Element Transcripts.** *The Journals of Gerontology: Series A* 2020,
1133 **76:805-810.**
- 1134 33. Sampathkumar NK, Bravo JI, Chen Y, Danthi PS, Donahue EK, Lai RW, Lu R, Randall
1135 LT, Vinson N, Benayoun BA: **Widespread sex dimorphism in aging and age-related**
1136 **diseases.** *Hum Genet* 2020, **139:333-356.**

- 1137 34. Baeken MW, Moosmann B, Hajjeva P: **Retrotransposon activation by distressed**
1138 **mitochondria in neurons.** *Biochemical and Biophysical Research Communications*
1139 2020, **525**:570-575.
- 1140 35. Valdebenito-Maturana B, Valdebenito-Maturana F, Carrasco M, Tapia JC, Maureira A:
1141 **Activation of Transposable Elements in Human Skeletal Muscle Fibers upon Statin**
1142 **Treatment.** *International Journal of Molecular Sciences* 2023, **24**:244.
- 1143 36. Tiwari B, Jones AE, Caillet CJ, Das S, Royer SK, Abrams JM: **p53 directly represses**
1144 **human LINE1 transposons.** *Genes & Development* 2020, **34**:1439-1451.
- 1145 37. Ardeljan D, Steranka JP, Liu C, Li Z, Taylor MS, Taylor MS, Payer LM, Gorbounov M,
1146 Sarnecki JS, Deshpande V, et al: **Cell fitness screens reveal a conflict between**
1147 **LINE-1 retrotransposition and DNA replication.** *Nature structural & molecular*
1148 *biology* 2020, **27**:168-178.
- 1149 38. Luqman-Fatah A, Watanabe Y, Uno K, Ishikawa F, Moran JV, Miyoshi T: **The interferon**
1150 **stimulated gene-encoded protein HELZ2 inhibits human LINE-1 retrotransposition**
1151 **and LINE-1 RNA-mediated type I interferon induction.** *Nature Communications* 2023,
1152 **14**:203.
- 1153 39. The EPC: **A User's Guide to the Encyclopedia of DNA Elements (ENCODE).** *PLOS*
1154 *Biology* 2011, **9**:e1001046.
- 1155 40. **An integrated encyclopedia of DNA elements in the human genome.** *Nature* 2012,
1156 **489**:57-74.
- 1157 41. Center DM, Cruikshank W: **Modulation of lymphocyte migration by human**
1158 **lymphokines. I. Identification and characterization of chemoattractant activity for**
1159 **lymphocytes from mitogen-stimulated mononuclear cells.** *J Immunol* 1982,
1160 **128**:2563-2568.
- 1161 42. Cruikshank WW, Center DM, Nisar N, Wu M, Natke B, Theodore AC, Kornfeld H:
1162 **Molecular and functional analysis of a lymphocyte chemoattractant factor:**

- 1163 **association of biologic function with CD4 expression.** *Proc Natl Acad Sci U S A*
1164 1994, **91**:5109-5113.
- 1165 43. Theodore AC, Center DM, Nicoll J, Fine G, Kornfeld H, Cruikshank WW: **CD4 ligand IL-**
1166 **16 inhibits the mixed lymphocyte reaction.** *J Immunol* 1996, **157**:1958-1964.
- 1167 44. Cruikshank WW, Lim K, Theodore AC, Cook J, Fine G, Weller PF, Center DM: **IL-16**
1168 **inhibition of CD3-dependent lymphocyte activation and proliferation.** *J Immunol*
1169 1996, **157**:5240-5248.
- 1170 45. Center DM, Kornfeld H, Cruikshank WW: **Interleukin 16 and its function as a CD4**
1171 **ligand.** *Immunol Today* 1996, **17**:476-481.
- 1172 46. Wilson KC, Center DM, Cruikshank WW: **Mini ReviewThe Effect of Interleukin-16 and**
1173 **its Precursor on T Lymphocyte Activation and Growth.** *Growth Factors* 2004, **22**:97-
1174 104.
- 1175 47. Huang Y, Du KL, Guo PY, Zhao RM, Wang B, Zhao XL, Zhang CQ: **IL-16 regulates**
1176 **macrophage polarization as a target gene of mir-145-3p.** *Mol Immunol* 2019, **107**:1-
1177 9.
- 1178 48. Rodriguez-Agudo D, Malacrida L, Kakiyama G, Sparrer T, Fortes C, Maceyka M, Subler
1179 MA, Windle JJ, Gratton E, Pandak WM, Gil G: **StarD5: an ER stress protein regulates**
1180 **plasma membrane and intracellular cholesterol homeostasis.** *Journal of Lipid*
1181 *Research* 2019, **60**:1087-1098.
- 1182 49. Rodriguez-Agudo D, Calderon-Dominguez M, Medina MA, Ren S, Gil G, Pandak WM:
1183 **ER stress increases StarD5 expression by stabilizing its mRNA and leads to**
1184 **relocalization of its protein from the nucleus to the membranes.** *J Lipid Res* 2012,
1185 **53**:2708-2715.
- 1186 50. Soccio RE, Adams RM, Maxwell KN, Breslow JL: **Differential Gene Regulation of**
1187 **StarD4 and StarD5 Cholesterol Transfer Proteins: ACTIVATION OF StarD4 BY**
1188 **STEROL REGULATORY ELEMENT-BINDING PROTEIN-2 AND StarD5 BY**

- 1189 **ENDOPLASMIC RETICULUM STRESS** *. *Journal of Biological Chemistry* 2005,
1190 **280**:19410-19418.
- 1191 51. Luu-The V, Tremblay P, Labrie F: **Characterization of type 12 17beta-hydroxysteroid**
1192 **dehydrogenase, an isoform of type 3 17beta-hydroxysteroid dehydrogenase**
1193 **responsible for estradiol formation in women.** *Mol Endocrinol* 2006, **20**:437-443.
- 1194 52. Heikelä H, Ruohonen ST, Adam M, Viitanen R, Liljenbäck H, Eskola O, Gabriel M,
1195 Mairinoja L, Pessia A, Velagapudi V, et al: **Hydroxysteroid (17β) dehydrogenase 12 is**
1196 **essential for metabolic homeostasis in adult mice.** *Am J Physiol Endocrinol Metab*
1197 2020, **319**:E494-e508.
- 1198 53. Nagasaki S, Miki Y, Akahira J, Suzuki T, Sasano H: **Transcriptional regulation of**
1199 **17beta-hydroxysteroid dehydrogenase type 12 by SREBP-1.** *Mol Cell Endocrinol*
1200 2009, **307**:163-168.
- 1201 54. Didier C, Broday L, Bhoumik A, Israeli S, Takahashi S, Nakayama K, Thomas SM,
1202 Turner CE, Henderson S, Sabe H, Ronai Ze: **RNF5, a RING Finger Protein That**
1203 **Regulates Cell Motility by Targeting Paxillin Ubiquitination and Altered**
1204 **Localization.** *Molecular and Cellular Biology* 2003, **23**:5331-5345.
- 1205 55. Tcherpakov M, Delaunay A, Toth J, Kadoya T, Petroski MD, Ronai ZeA: **Regulation of**
1206 **Endoplasmic Reticulum-associated Degradation by RNF5-dependent**
1207 **Ubiquitination of JNK-associated Membrane Protein (JAMP)** *. *Journal of Biological*
1208 *Chemistry* 2009, **284**:12099-12109.
- 1209 56. Zhong B, Zhang Y, Tan B, Liu TT, Wang YY, Shu HB: **The E3 ubiquitin ligase RNF5**
1210 **targets virus-induced signaling adaptor for ubiquitination and degradation.** *J*
1211 *Immunol* 2010, **184**:6249-6255.
- 1212 57. Zhong B, Zhang L, Lei C, Li Y, Mao A-P, Yang Y, Wang Y-Y, Zhang X-L, Shu H-B: **The**
1213 **Ubiquitin Ligase RNF5 Regulates Antiviral Responses by Mediating Degradation**
1214 **of the Adaptor Protein MITA.** *Immunity* 2009, **30**:397-407.

- 1215 58. Lai RW, Lu R, Danthi PS, Bravo JI, Goumba A, Sampathkumar NK, Benayoun BA:
1216 **Multi-level remodeling of transcriptional landscapes in aging and longevity.** *BMB*
1217 *Rep* 2019, **52**:86-108.
- 1218 59. Sato S, Gillette M, de Santiago PR, Kuhn E, Burgess M, Doucette K, Feng Y, Mendez-
1219 Dorantes C, Ippoliti PJ, Hobday S, et al: **LINE-1 ORF1p as a candidate biomarker in**
1220 **high grade serous ovarian carcinoma.** *Scientific Reports* 2023, **13**:1537.
- 1221 60. Rodić N, Sharma R, Sharma R, Zampella J, Dai L, Taylor MS, Hruban RH, Iacobuzio-
1222 Donahue CA, Maitra A, Torbenson MS, et al: **Long Interspersed Element-1 Protein**
1223 **Expression Is a Hallmark of Many Human Cancers.** *The American Journal of*
1224 *Pathology* 2014, **184**:1280-1286.
- 1225 61. Lindholm HT, Chen R, De Carvalho DD: **Endogenous retroelements as alarms for**
1226 **disruptions to cellular homeostasis.** *Trends in Cancer* 2023, **9**:55-68.
- 1227 62. Jeck WR, Siebold AP, Sharpless NE: **Review: a meta-analysis of GWAS and age-**
1228 **associated diseases.** *Aging Cell* 2012, **11**:727-731.
- 1229 63. Ramirez J, Bitterman P, Basu S, Barua A: **Changes in IL-16 Expression in the Ovary**
1230 **during Aging and Its Potential Consequences to Ovarian Pathology.** *J Immunol Res*
1231 2022, **2022**:2870389.
- 1232 64. Lonsdale J, Thomas J, Salvatore M, Phillips R, Lo E, Shad S, Hasz R, Walters G, Garcia
1233 F, Young N, et al: **The Genotype-Tissue Expression (GTEx) project.** *Nature Genetics*
1234 2013, **45**:580-585.
- 1235 65. Carithers LJ, Ardlie K, Barcus M, Branton PA, Britton A, Buia SA, Compton CC, DeLuca
1236 DS, Peter-Demchok J, Gelfand ET, et al: **A Novel Approach to High-Quality**
1237 **Postmortem Tissue Procurement: The GTEx Project.** *Biopreservation and*
1238 *Biobanking* 2015, **13**:311-319.

- 1239 66. Streeter I, Harrison PW, Faulconbridge A, The HipSci Consortium, Flicek P, Parkinson
1240 H, Clarke L: **The human-induced pluripotent stem cell initiative—data resources for**
1241 **cellular genetics.** *Nucleic Acids Research* 2016, **45**:D691-D697.
- 1242 67. Chick JM, Munger SC, Simecek P, Huttlin EL, Choi K, Gatti DM, Raghupathy N,
1243 Svenson KL, Churchill GA, Gygi SP: **Defining the consequences of genetic variation**
1244 **on a proteome-wide scale.** *Nature* 2016, **534**:500-505.
- 1245 68. Stegle O, Parts L, Piipari M, Winn J, Durbin R: **Using probabilistic estimation of**
1246 **expression residuals (PEER) to obtain increased power and interpretability of**
1247 **gene expression analyses.** *Nat Protoc* 2012, **7**:500-507.
- 1248 69. Leek JT: **svaseq: removing batch effects and other unwanted noise from**
1249 **sequencing data.** *Nucleic Acids Research* 2014, **42**:e161-e161.
- 1250 70. Savytska N, Heutink P, Bansal V: **Transcription start site signal profiling improves**
1251 **transposable element RNA expression analysis at locus-level.** *Frontiers in Genetics*
1252 2022, **13**.
- 1253 71. Lanciano S, Cristofari G: **Measuring and interpreting transposable element**
1254 **expression.** *Nature Reviews Genetics* 2020, **21**:721-736.
- 1255 72. Zeng TB, Pierce N, Liao J, Szabó PE: **H3K9 methyltransferase EHMT2/G9a controls**
1256 **ERVK-driven noncanonical imprinted genes.** *Epigenomics* 2021, **13**:1299-1314.
- 1257 73. Jiang Q, Ang JYJ, Lee AY, Cao Q, Li KY, Yip KY, Leung DCY: **G9a Plays Distinct**
1258 **Roles in Maintaining DNA Methylation, Retrotransposon Silencing, and Chromatin**
1259 **Looping.** *Cell Reports* 2020, **33**:108315.
- 1260 74. Rantakari P, Lagerbohm H, Kaimainen M, Suomela J-P, Strauss L, Sainio K, Pakarinen
1261 P, Poutanen M: **Hydroxysteroid (17 β) Dehydrogenase 12 Is Essential for Mouse**
1262 **Organogenesis and Embryonic Survival.** *Endocrinology* 2010, **151**:1893-1901.

- 1263 75. Garcia G, Zhang H, Moreno S, Tsui CK, Webster BM, Higuchi-Sanabria R, Dillin A:
1264 **Lipid homeostasis is essential for a maximal ER stress response.** *eLife* 2023,
1265 **12:e83884.**
- 1266 76. Baier M, Werner A, Bannert N, Metzner K, Kurth R: **HIV suppression by interleukin-**
1267 **16.** *Nature* 1995, **378**:563.
- 1268 77. Zhou P, Goldstein S, Devadas K, Tewari D, Notkins AL: **Human CD4+ cells**
1269 **transfected with IL-16 cDNA are resistant to HIV-1 infection: inhibition of mRNA**
1270 **expression.** *Nat Med* 1997, **3**:659-664.
- 1271 78. Idziorek T, Khalife J, Billaut-Mulot O, Hermann E, Aumercier M, Mouton Y, Capron A,
1272 Bahr GM: **Recombinant human IL-16 inhibits HIV-1 replication and protects against**
1273 **activation-induced cell death (AICD).** *Clin Exp Immunol* 1998, **112**:84-91.
- 1274 79. Jia R, Jiang C, Li L, Huang C, Lu L, Xu M, Xu J, Liang X: **Interleukin 16 Enhances the**
1275 **Host Susceptibility to Influenza A Virus Infection.** *Frontiers in Microbiology* 2021, **12.**
- 1276 80. Liu S, Lei Z, Li J, Wang L, Jia R, Liu Z, Jiang C, Gao Y, Liu M, Kuang L, et al:
1277 **Interleukin 16 contributes to gammaherpesvirus pathogenesis by inhibiting viral**
1278 **reactivation.** *PLoS Pathog* 2020, **16**:e1008701.
- 1279 81. Watanabe T, Watanabe S, Kawaoka Y: **Cellular Networks Involved in the Influenza**
1280 **Virus Life Cycle.** *Cell Host & Microbe* 2010, **7**:427-439.
- 1281 82. Germain MA, Chatel-Chaix L, Gagné B, Bonneil É, Thibault P, Pradezynski F, de
1282 Chasse B, Meyniel-Schicklin L, Lotteau V, Baril M, Lamarre D: **Elucidating novel**
1283 **hepatitis C virus-host interactions using combined mass spectrometry and**
1284 **functional genomics approaches.** *Mol Cell Proteomics* 2014, **13**:184-203.
- 1285 83. Mohamed B, Mazeaud C, Baril M, Poirier D, Sow AA, Chatel-Chaix L, Titorenko V,
1286 Lamarre D: **Very-long-chain fatty acid metabolic capacity of 17-beta-**
1287 **hydroxysteroid dehydrogenase type 12 (HSD17B12) promotes replication of**
1288 **hepatitis C virus and related flaviviruses.** *Scientific Reports* 2020, **10**:4040.

- 1289 84. Feng K, Min Y-Q, Sun X, Deng F, Li P, Wang H, Ning Y-J: **Interactome profiling**
1290 **reveals interaction of SARS-CoV-2 NSP13 with host factor STAT1 to suppress**
1291 **interferon signaling.** *Journal of Molecular Cell Biology* 2021, **13**:760-762.
- 1292 85. Yuan Z, Hu B, Xiao H, Tan X, Li Y, Tang K, Zhang Y, Cai K, Ding B: **The E3 Ubiquitin**
1293 **Ligase RNF5 Facilitates SARS-CoV-2 Membrane Protein-Mediated Virion Release.**
1294 *mBio* 2022, **13**:e03168-03121.
- 1295 86. Li Z, Hao P, Zhao Z, Gao W, Huan C, Li L, Chen X, Wang H, Jin N, Luo Z-Q, et al: **The**
1296 **E3 ligase RNF5 restricts SARS-CoV-2 replication by targeting its envelope protein**
1297 **for degradation.** *Signal Transduction and Targeted Therapy* 2023, **8**:53.
- 1298 87. Danecek P, Bonfield JK, Liddle J, Marshall J, Ohan V, Pollard MO, Whitwham A, Keane
1299 T, McCarthy SA, Davies RM, Li H: **Twelve years of SAMtools and BCFtools.**
1300 *GigaScience* 2021, **10**.
- 1301 88. Danecek P, Auton A, Abecasis G, Albers CA, Banks E, DePristo MA, Handsaker RE,
1302 Lunter G, Marth GT, Sherry ST, et al: **The variant call format and VCFtools.**
1303 *Bioinformatics* 2011, **27**:2156-2158.
- 1304 89. Gao F, Chang D, Biddanda A, Ma L, Guo Y, Zhou Z, Keinan A: **XWAS: A Software**
1305 **Toolset for Genetic Data Analysis and Association Studies of the X Chromosome.**
1306 *J Hered* 2015, **106**:666-671.
- 1307 90. Keur N, Ricaño-Ponce I, Kumar V, Matzaraki V: **A systematic review of analytical**
1308 **methods used in genetic association analysis of the X-chromosome.** *Briefings in*
1309 *Bioinformatics* 2022, **23**.
- 1310 91. Purcell S, Neale B, Todd-Brown K, Thomas L, Ferreira MAR, Bender D, Maller J, Sklar
1311 P, de Bakker PIW, Daly MJ, Sham PC: **PLINK: A Tool Set for Whole-Genome**
1312 **Association and Population-Based Linkage Analyses.** *The American Journal of*
1313 *Human Genetics* 2007, **81**:559-575.

- 1314 92. Ahl V, Keller H, Schmidt S, Weichenrieder O: **Retrotransposition and Crystal**
1315 **Structure of an Alu RNP in the Ribosome-Stalling Conformation.** *Molecular Cell*
1316 2015, **60**:715-727.
- 1317 93. Chen S, Zhou Y, Chen Y, Gu J: **fastp: an ultra-fast all-in-one FASTQ preprocessor.**
1318 *Bioinformatics* 2018, **34**:i884-i890.
- 1319 94. Frankish A, Diekhans M, Ferreira A-M, Johnson R, Jungreis I, Loveland J, Mudge JM,
1320 Sisu C, Wright J, Armstrong J, et al: **GENCODE reference annotation for the human**
1321 **and mouse genomes.** *Nucleic Acids Research* 2018, **47**:D766-D773.
- 1322 95. Dobin A, Davis CA, Schlesinger F, Drenkow J, Zaleski C, Jha S, Batut P, Chaisson M,
1323 Gingeras TR: **STAR: ultrafast universal RNA-seq aligner.** *Bioinformatics* 2012, **29**:15-
1324 21.
- 1325 96. Love MI, Huber W, Anders S: **Moderated estimation of fold change and dispersion**
1326 **for RNA-seq data with DESeq2.** *Genome Biology* 2014, **15**:550.
- 1327 97. Ritchie ME, Phipson B, Wu D, Hu Y, Law CW, Shi W, Smyth GK: **limma powers**
1328 **differential expression analyses for RNA-sequencing and microarray studies.**
1329 *Nucleic Acids Research* 2015, **43**:e47-e47.
- 1330 98. Macchietto MG, Langlois RA, Shen SS: **Virus-induced transposable element**
1331 **expression up-regulation in human and mouse host cells.** *Life Sci Alliance* 2020, **3**.
- 1332 99. Shabalin AA: **Matrix eQTL: ultra fast eQTL analysis via large matrix operations.**
1333 *Bioinformatics* 2012, **28**:1353-1358.
- 1334 100. Wang T, Peng Q, Liu B, Liu X, Liu Y, Peng J, Wang Y: **eQTLMAPT: Fast and Accurate**
1335 **eQTL Mediation Analysis With Efficient Permutation Testing Approaches.** *Frontiers*
1336 *in Genetics* 2020, **10**.
- 1337 101. Wu T, Hu E, Xu S, Chen M, Guo P, Dai Z, Feng T, Zhou L, Tang W, Zhan L, et al:
1338 **clusterProfiler 4.0: A universal enrichment tool for interpreting omics data.** *The*
1339 *Innovation* 2021, **2**:100141.

- 1340 102. Ghossaini M, Mountjoy E, Carmona M, Peat G, Schmidt EM, Hercules A, Fumis L,
1341 Miranda A, Carvalho-Silva D, Buniello A, et al: **Open Targets Genetics: systematic**
1342 **identification of trait-associated genes using large-scale genetics and functional**
1343 **genomics.** *Nucleic Acids Res* 2021, **49**:D1311-d1320.
- 1344 103. Kim S-S, Hudgins AD, Gonzalez B, Milman S, Barzilai N, Vijg J, Tu Z, Suh Y: **A**
1345 **Compendium of Age-Related PheWAS and GWAS Traits for Human Genetic**
1346 **Association Studies, Their Networks and Genetic Correlations.** *Frontiers in*
1347 *Genetics* 2021, **12**.
- 1348
- 1349
- 1350

1351 **FIGURE LEGENDS**

1352

1353 **Figure 1. Overview of the pipeline developed to scan for L1 transcriptional**
1354 **regulators *in silico*.**

1355 **(A)** An illustration of the samples and “omic” data used in this study. Of the 358
1356 European individuals, 187 were female and 171 were male. Of the 86 African
1357 individuals, 49 were female and 37 were male. (Note that Utah subjects are of Northern
1358 European ancestry, and thus part of the European cohort for analytical purposes). **(B)** A
1359 schematic illustrating how genetic variants, gene expression, and TE expression can be
1360 integrated to identify highly correlated SNV-Gene-TE trios. **(C)** A Manhattan plot for the
1361 L1 subfamily *trans*-eQTL analysis in the European cohort. The genes that passed our
1362 three-part integration approach are listed next to the most significant *trans*-eQTL SNV
1363 they were associated with in *cis*. The dashed line at $p = 3.44E-8$ corresponds to an
1364 average empirical FDR < 0.05 , based on 20 random permutations. One such
1365 permutation is illustrated in the bottom panel. The solid line at $p = 2.31E-8$ corresponds
1366 to a Benjamini-Hochberg FDR < 0.05 . The stricter of the two thresholds, $p = 2.31E-8$,
1367 was used to define significant *trans*-eQTLs. FDR: False Discovery Rate. Some panels
1368 were created with BioRender.com.

1369

1370 **Figure 2. Identification of 1st tier candidate L1 expression regulators in the**
1371 **European cohort.**

1372 **(A)** A schematic for how 1st tier candidate genes were defined. In short, these were
1373 genes in trios with index SNVs that were at the top of their respective peak. **(B)** The

1374 three-part integration results for three protein-coding genes—*STARD5*, *IL16*,
1375 *HSD17B12*—that we considered first tier candidates for functional, *in vitro* testing. In the
1376 left column are the *trans*-eQTLs, in the middle column are the *cis*-eQTLs, and in the
1377 right column are the linear regressions for gene expression against L1 subfamily
1378 expression. Expression values following an inverse normal transform (INT) are shown.
1379 The FDR for each analysis is listed at the top of each plot. FDR: False Discovery Rate.

1380

1381 **Figure 3. L1 *trans*-eQTLs are associated with subtle, widespread differences in TE**
1382 **families and known TE-associated pathways.**

1383 **(A)** Scheme for functionally annotating gene-linked index SNVs by GSEA. **(B)** GSEA
1384 analysis for shared, significantly regulated TE family gene sets across genotypes for
1385 rs11635336 (*IL16/STARD5*), rs9271894 (*HLA*), and rs1061810 (*HSD17B12*). **(C)** GSEA
1386 plots for the L1 family gene set results summarized in **(B)**. For these plots, the FDR
1387 value is listed. GSEA analysis for top, shared, concomitantly regulated **(D)** MSigDB
1388 Hallmark pathway, **(E)** GO Biological Process, and **(F)** Reactome pathway gene sets
1389 across genotypes for rs11635336 (*IL16/STARD5*), rs9271894 (*HLA*), and rs1061810
1390 (*HSD17B12*). Shared gene sets were ranked by combining p-values from each
1391 individual SNV analysis using Fisher's method. In each bubble plot, the size of the dot
1392 represents the $-\log_{10}(\text{FDR})$ and the color reflects the normalized enrichment score.
1393 FDR: False Discovery Rate.

1394

1395 **Figure 4. Impact of *IL16* and *STARD5* overexpression on LCL gene and TE**
1396 **expression landscapes.**

1397 *IL16* and *STARD5* overexpression induce changes consistent with their known biology,
1398 as well as subtle but widespread upregulation of TE families. **(A)** Scheme for
1399 experimentally validating the roles of *IL16* and *STARD5* in L1 regulation. GSEA analysis
1400 for top, differentially regulated **(B)** GO Biological Process and **(C)** Reactome pathway
1401 gene sets following *IL16* overexpression. GSEA analysis for top, differentially regulated
1402 **(D)** GO Biological Process and **(E)** Reactome pathway gene sets following *STARD5*
1403 overexpression. **(F)** GSEA analysis for shared, significantly regulated TE family gene
1404 sets following *IL16* and *STARD5* overexpression. **(G)** GSEA plots for the L1 family gene
1405 set results summarized in **(F)**. For these plots, the FDR value is listed. In each bubble
1406 plot, the size of the dot represents the $-\log_{10}(\text{FDR})$ and the color reflects the normalized
1407 enrichment score. FDR: False Discovery Rate. Some panels were created with
1408 BioRender.com.

1409

1410 **Figure 5. rhIL16 treatment is sufficient to transiently upregulate an L1 family gene**
1411 **set.**

1412 **(A)** Scheme for experimentally validating the role of rhIL16 in L1 regulation. GSEA
1413 analysis for top, shared, concomitantly regulated **(B)** GO Biological Process and **(C)**
1414 Reactome pathway gene sets following *IL16* overexpression and rhIL16 exposure for 24
1415 hours. Shared gene sets were ranked by combining p-values from each individual
1416 treatment analysis using Fisher's method. **(D)** GSEA analysis for top, differentially
1417 regulated TE family gene sets following rhIL16 exposure for 24 hours. The GSEA plot
1418 for the L1 family gene set result summarized in the bubble plot is also shown. For this
1419 plot, the FDR value is listed. In each bubble plot, the size of the dot represents the -

1420 $\log_{10}(\text{FDR})$ and the color reflects the normalized enrichment score. FDR: False
1421 Discovery Rate. Some panels were created with BioRender.com.

1422

1423 **Figure 6. Consistent cellular responses to *IL16* overexpression, *STARD5***
1424 **overexpression, and rhIL16 exposure for 24 hours.**

1425 *IL16* overexpression, *STARD5* overexpression, and rhIL16 exposure for 24 hours are
1426 associated with subtle but widespread differences in TE families and known TE-
1427 associated pathways. **(A)** Scheme for assessing concordantly regulated TE family and
1428 pathway gene sets across conditions where an L1 gene set is upregulated. GSEA
1429 analysis for top, shared, concomitantly regulated **(B)** TE family, **(C)** MSigDB Hallmark
1430 pathway, **(D)** GO Biological Process, and **(E)** Reactome pathway gene sets following
1431 *IL16* overexpression, *STARD5* overexpression, and rhIL16 exposure for 24 hours.
1432 Shared gene sets were ranked by combining p-values from each individual treatment
1433 analysis using Fisher's method. In each bubble plot, the size of the dot represents the -
1434 $\log_{10}(\text{FDR})$ and the color reflects the normalized enrichment score. FDR: False
1435 Discovery Rate.

1436

1437 **Figure 7. L1 *trans*-eQTLs are co-associated with aging traits in GWAS databases.**

1438 **(A)** Scheme for obtaining *trans*-eQTL SNV-associated aging phenotypes from the Open
1439 Targets Genetics platform. **(B)** A pie chart representing the number of SNVs (222/499)
1440 associated with an aging-related MeSH trait, either by PheWAS or indirectly linked to
1441 the phenotype through a proxy lead SNP in LD with the SNV. **(C)** Histogram depicting
1442 the distribution of number of aging MeSH traits associated with the 222/499 SNVs by

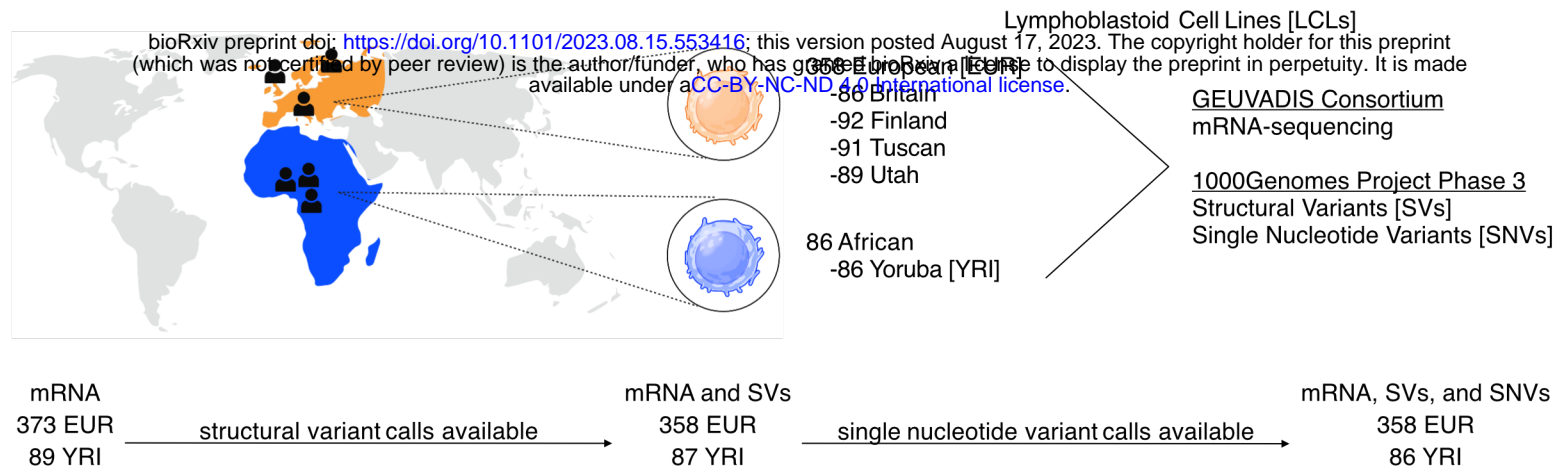
1443 PheWAS. **(D)** Histogram depicting the distribution of number of aging MeSH traits linked
1444 with the 222/499 SNVs through a proxy lead SNP in LD with the SNVs. **(E)** A diagram
1445 highlighting the organ targets of the top 10 most frequently associated aging traits. **(F)**
1446 The concentrations of circulating IL16 in aging mice of both sexes was assessed by
1447 ELISA. Significance across age in each sex was assessed using a Wilcoxon test. The
1448 p-values from each sex (females in pink and males in blue) were combined by meta-
1449 analysis using Fisher's method. Any p-value < 0.05 was considered significant. Some
1450 panels were created with BioRender.com.

1451

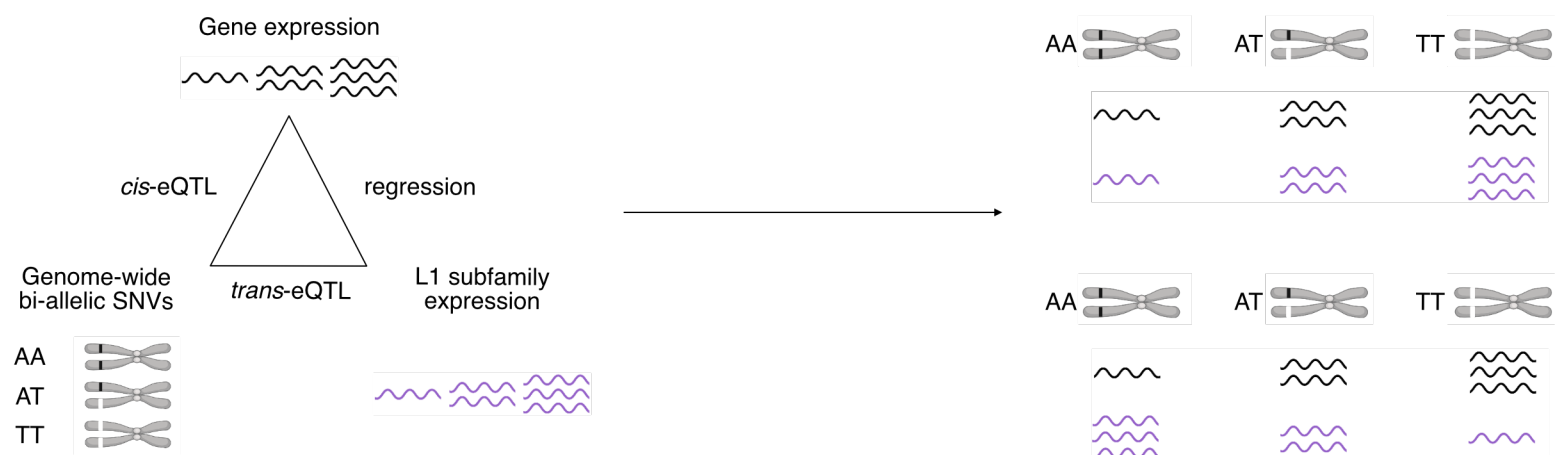
1452

Figure 1

A Samples and data used in this study



B Scheme for *in silico* identification of candidate transposon-subfamily regulators



C Manhattan plots for European L1 *trans*-eQTL analysis

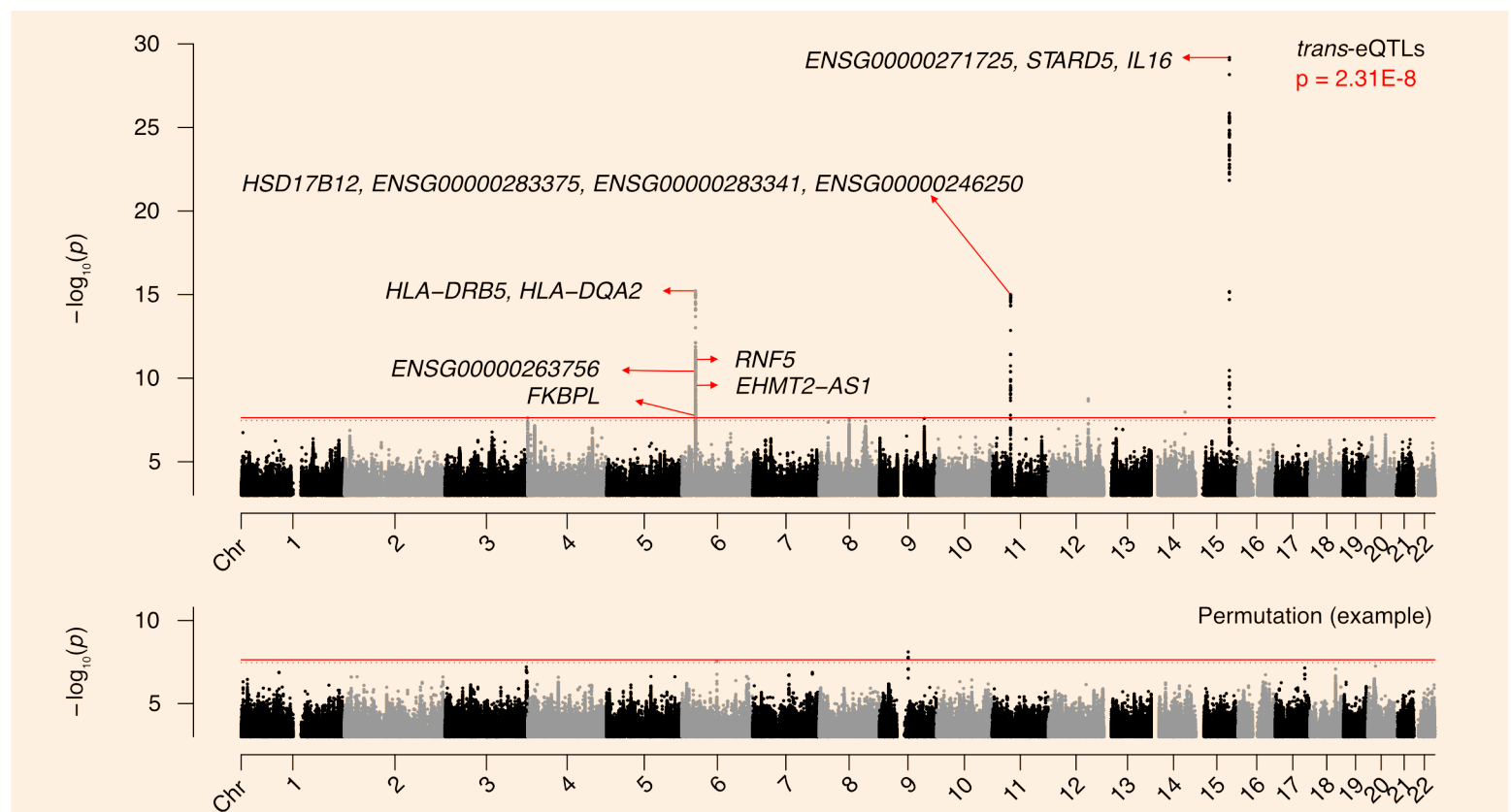
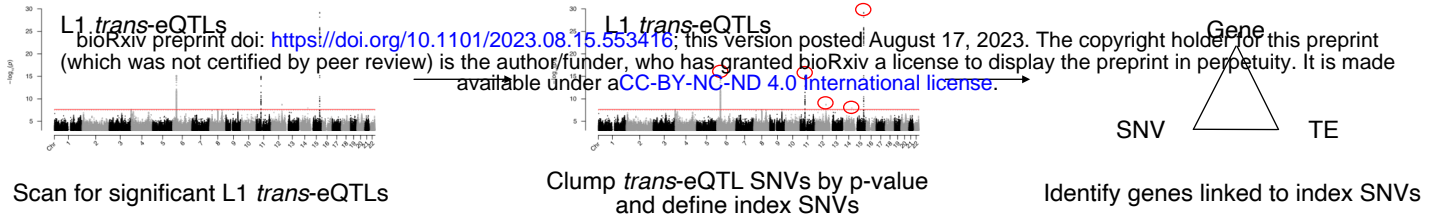


Figure 2

A Scheme for defining 1st tier candidate genes



B *In silico* screen results for 1st tier candidate regulators

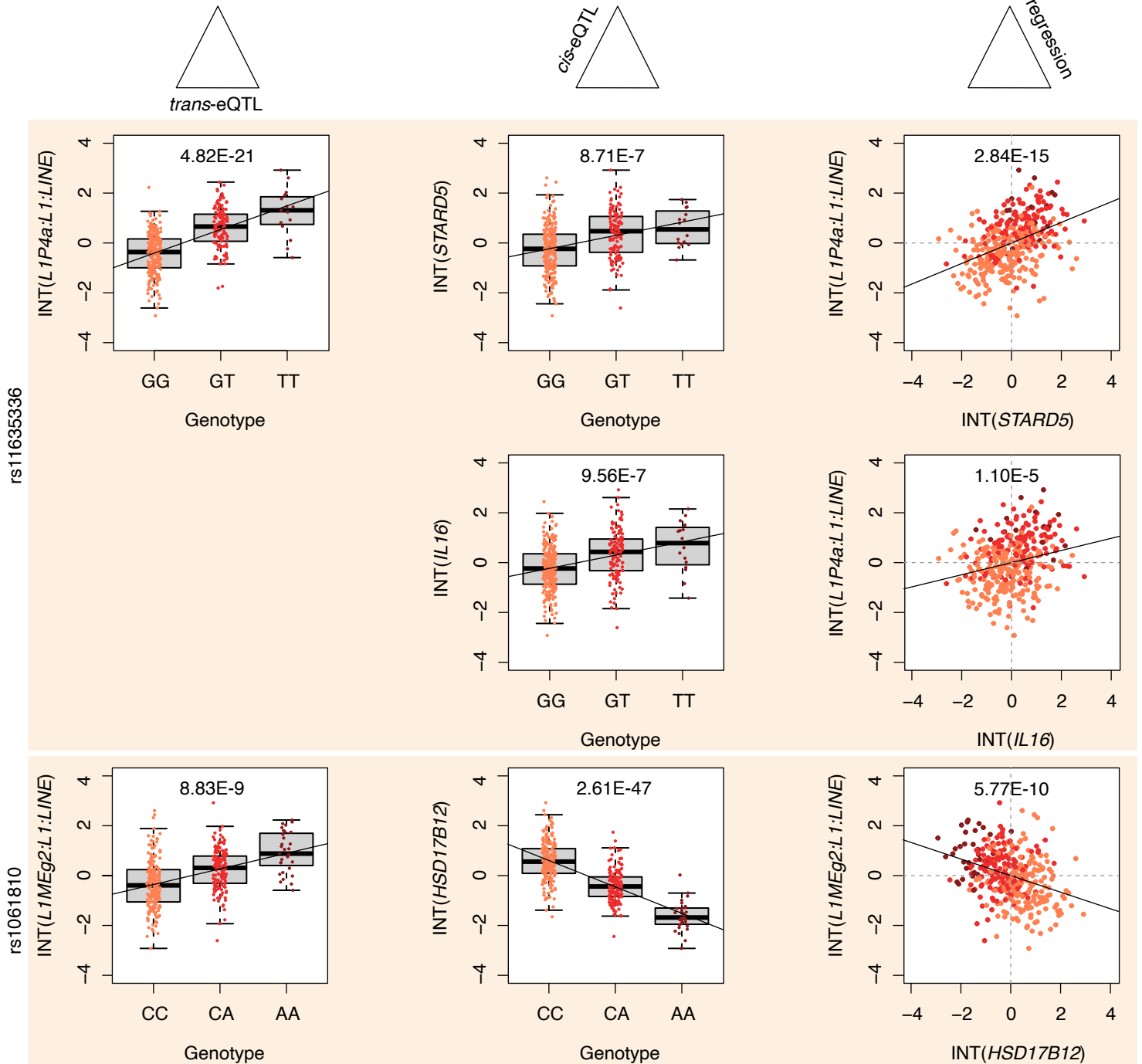
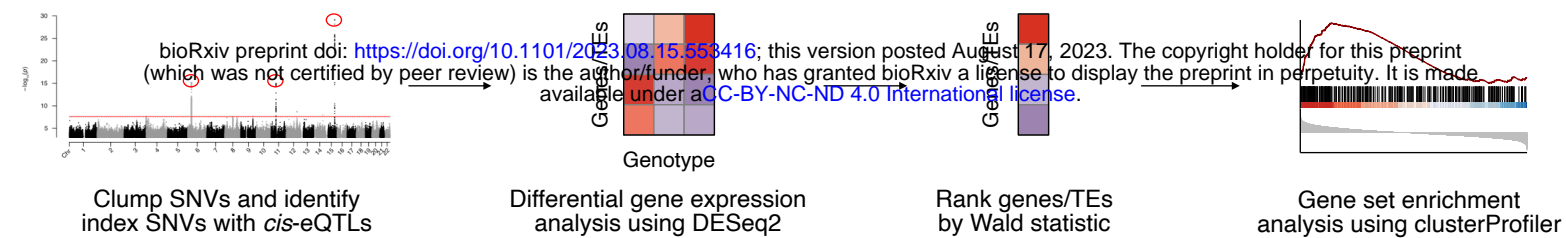
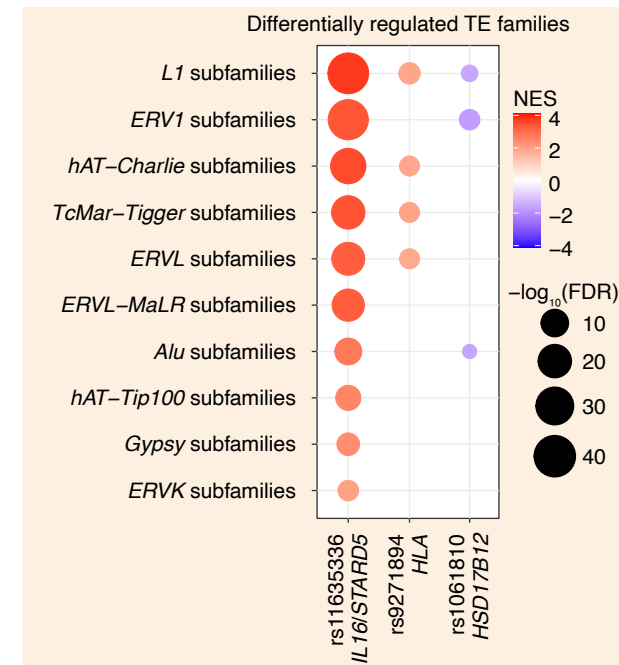


Figure 3

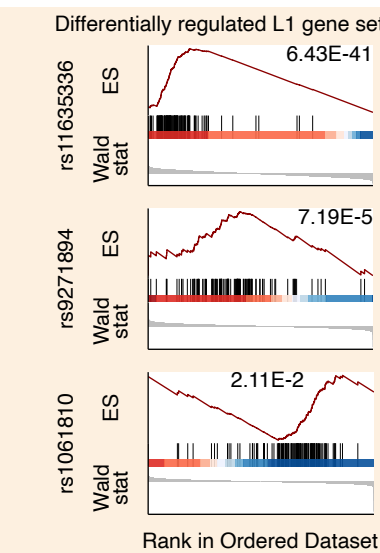
A Scheme for functionally annotating SNVs



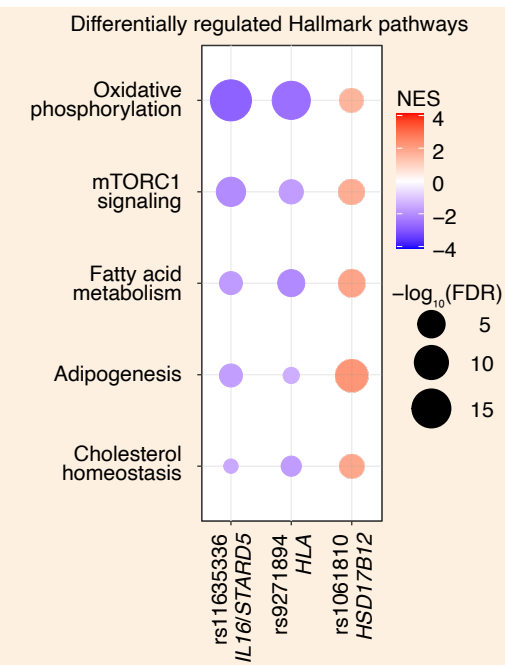
B Index SNV associations with TE family gene sets



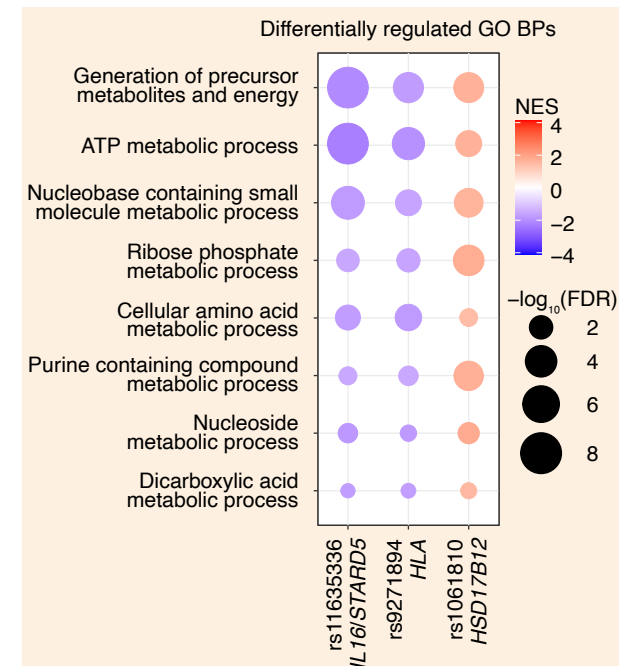
C Index SNV associations with an L1 family gene set



D Index SNV associations with MSigDB Hallmark gene sets



E Index SNV associations with GO Biological Process gene sets



F Index SNV associations with Reactome gene sets

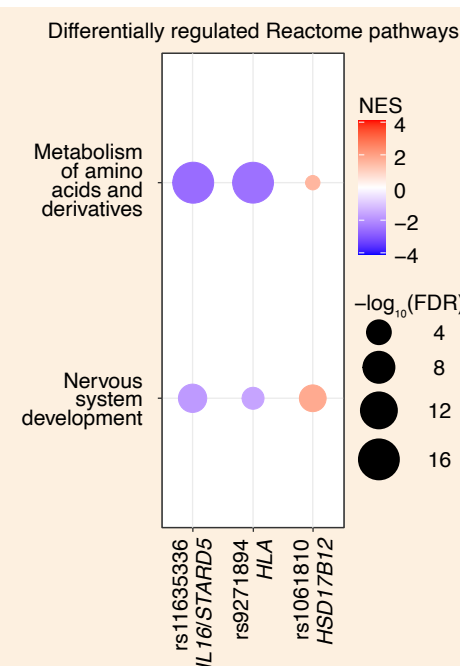
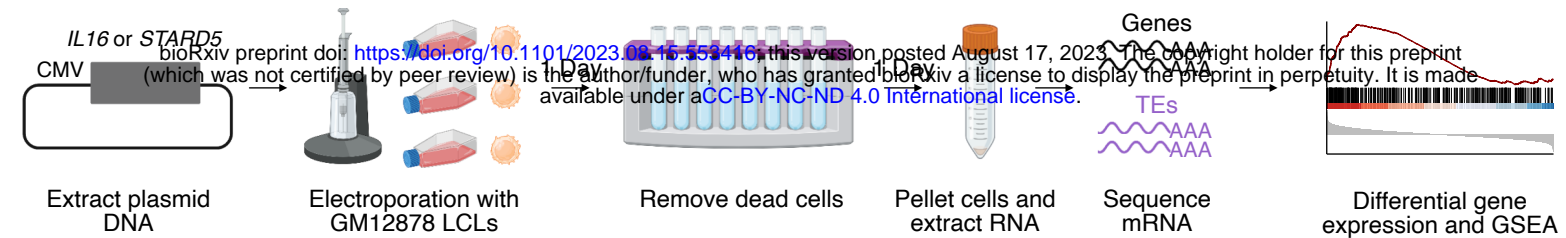
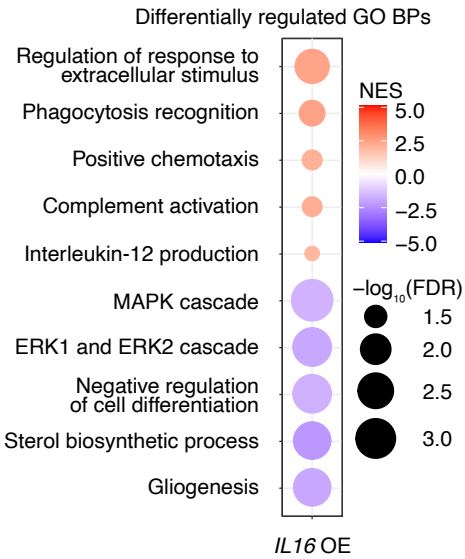


Figure 4

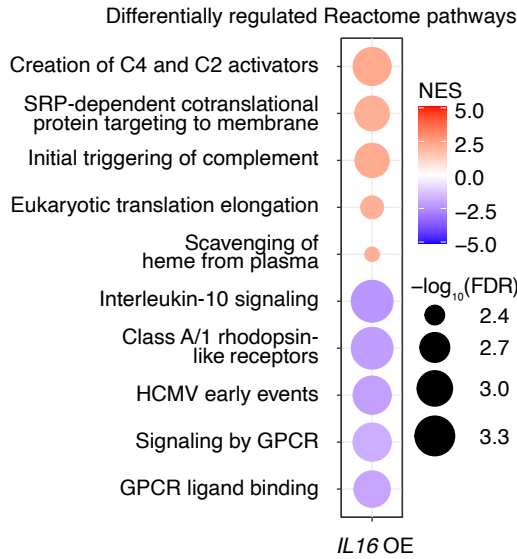
A Scheme for assessing the effects of candidate genes on L1 expression



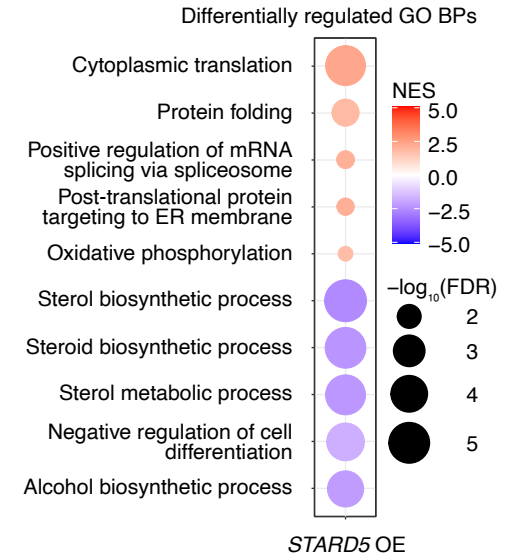
B Top enriched GO Biological Processes following *IL16* overexpression



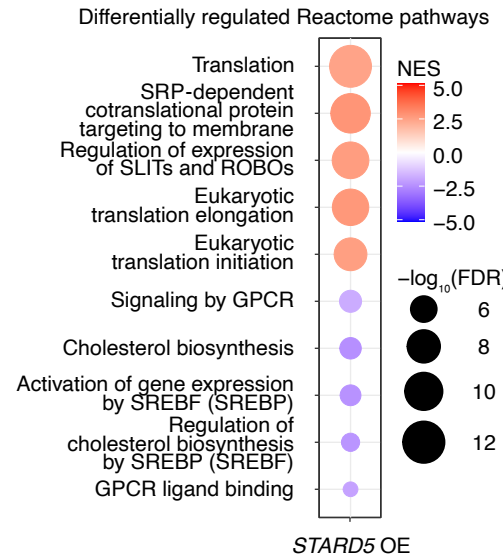
C Top enriched Reactome gene sets following *IL16* overexpression



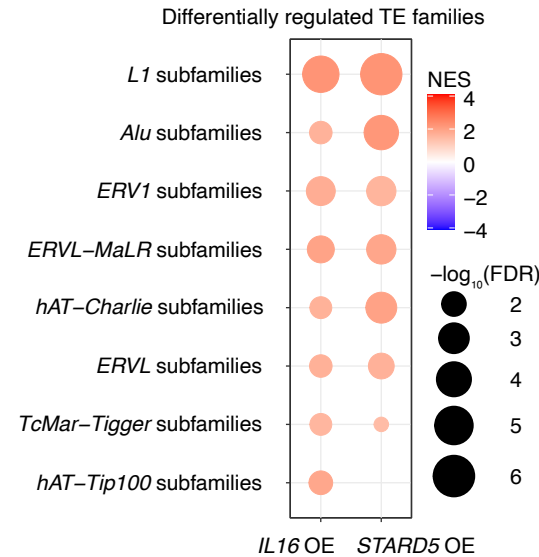
D Top enriched GO Biological Processes following *STARD5* overexpression



E Top enriched Reactome gene sets following *STARD5* overexpression



F *IL16* and *STARD5* associations with TE family gene sets



G *IL16* and *STARD5* associations with an L1 family gene set

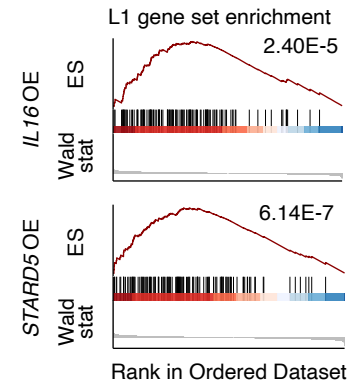
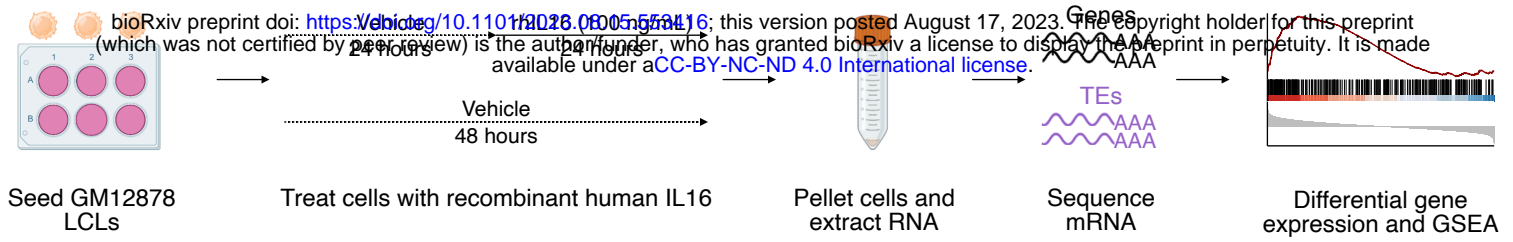
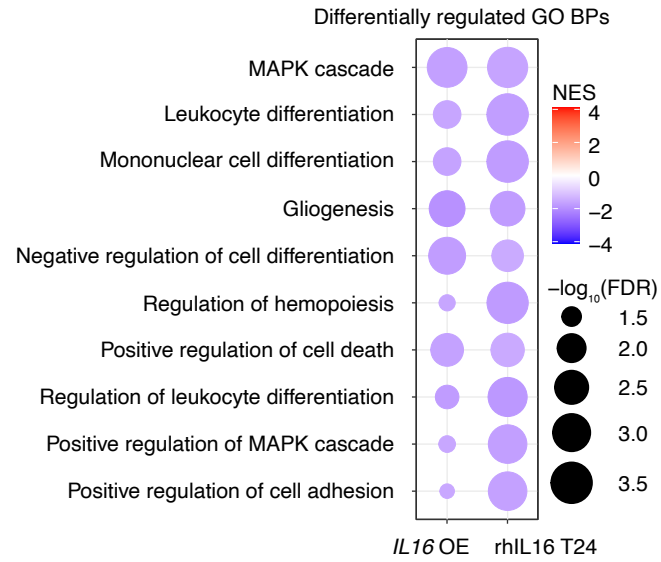


Figure 5

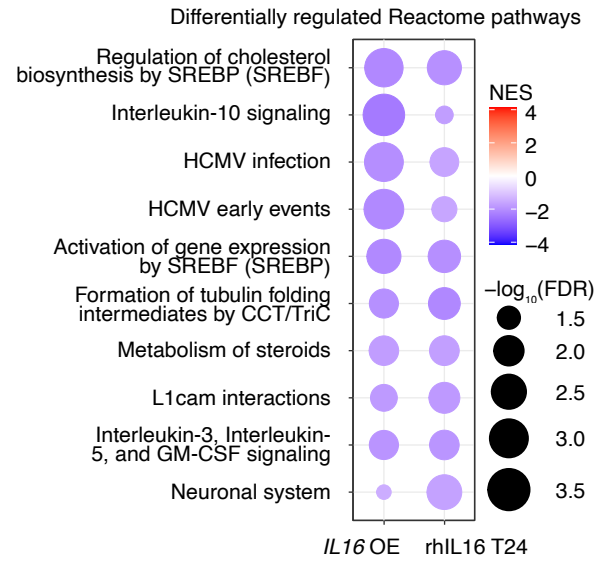
A Scheme for assessing the effects of IL16 protein on L1 expression



B Top shared GO Biological Processes



C Top shared Reactome gene sets



D rhIL16 associations with TE family gene sets

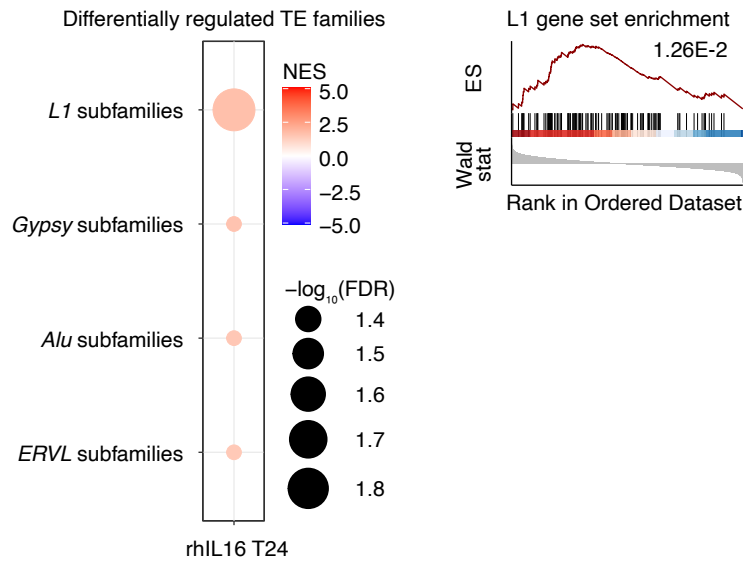
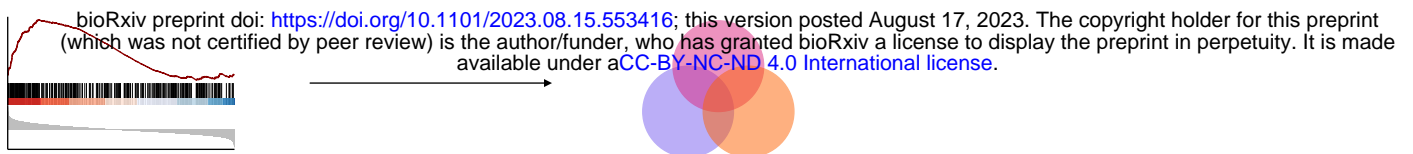


Figure 6

A Scheme for assessing shared pathway changes in conditions with L1 regulation

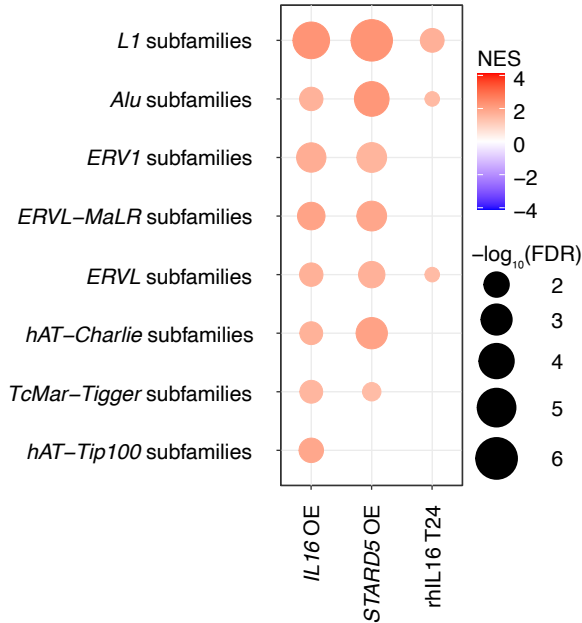


GSEA for experimental conditions with L1 regulation

Identify common pathways

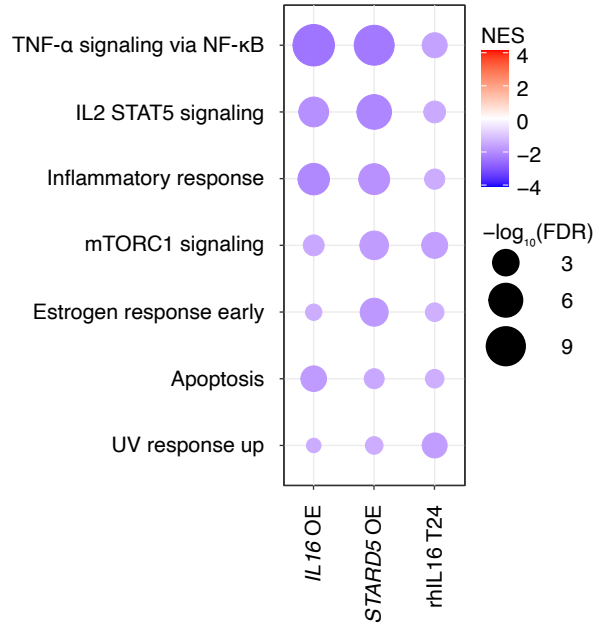
B Shared upregulated TE family gene sets

Differentially regulated TE families



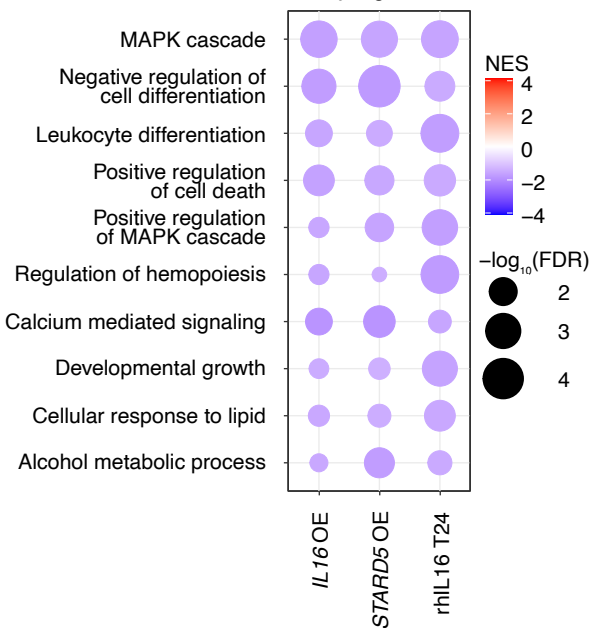
C Top shared Hallmark pathways

Differentially regulated Hallmark pathways



D Top shared GO Biological Processes

Differentially regulated GO BPs



E Top shared Reactome pathways

Differentially regulated Reactome pathways

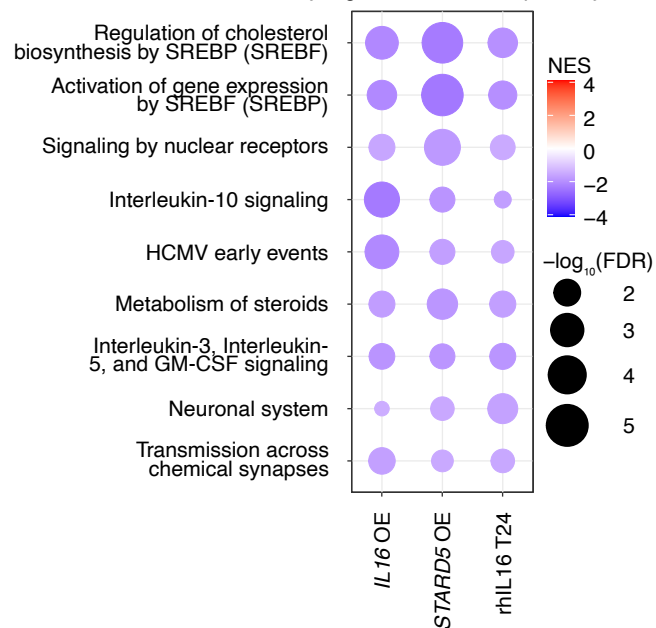
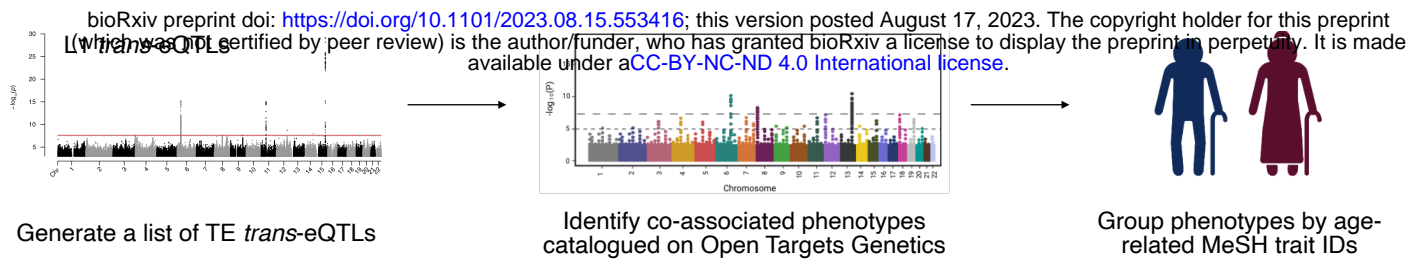
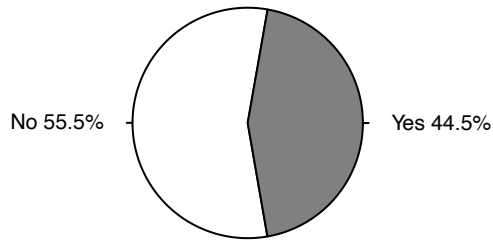


Figure 7

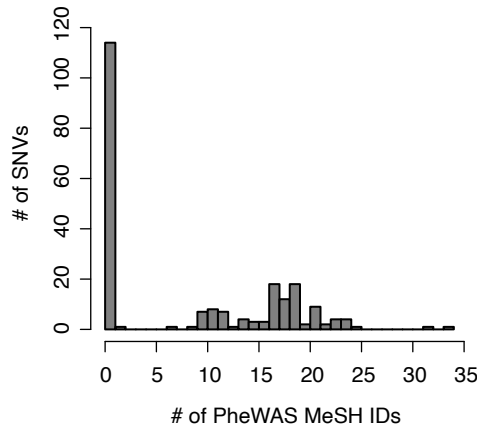
A Scheme for identifying TE eQTL co-associated aging traits



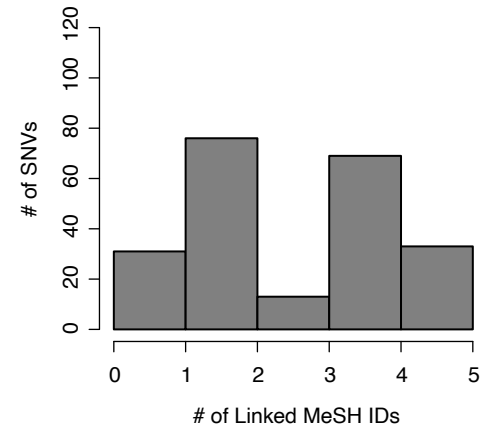
B Number of SNVs with an age-related MeSH trait



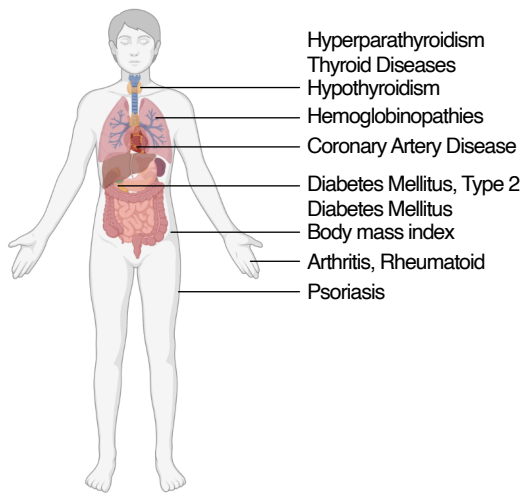
C Number of associated age-related traits per SNV



D Number of linked age-related traits per SNV



E Top traits with the most number of associated SNVs



F Mouse serum [IL16] with age

